



**HAL**  
open science

## **Piezo1 is required for outflow tract and aortic valve development.**

Adèle Faucherre, Hamid Moha Ou Maati, Nathalie Nasr, Amélie Pinard, Alexis Theron, Gaëlle Odelin, Jean-Pierre Desvignes, David Salgado, Gwenaëlle Collod-Beroud, Jean-François Avierinos, et al.

► **To cite this version:**

Adèle Faucherre, Hamid Moha Ou Maati, Nathalie Nasr, Amélie Pinard, Alexis Theron, et al.. Piezo1 is required for outflow tract and aortic valve development.. *Journal of Molecular and Cellular Cardiology*, 2020, 143, pp.51-62. 10.1016/j.yjmcc.2020.03.013 . hal-02863713

**HAL Id: hal-02863713**

**<https://hal.science/hal-02863713v1>**

Submitted on 11 Nov 2020

**HAL** is a multi-disciplinary open access archive for the deposit and dissemination of scientific research documents, whether they are published or not. The documents may come from teaching and research institutions in France or abroad, or from public or private research centers.

L'archive ouverte pluridisciplinaire **HAL**, est destinée au dépôt et à la diffusion de documents scientifiques de niveau recherche, publiés ou non, émanant des établissements d'enseignement et de recherche français ou étrangers, des laboratoires publics ou privés.

1  
2 **Piezo1 is required for zebrafish outflow tract and**  
3 **aortic valve development.**

4 (Piezo1 and outflow tract/aortic valve development)

5 †*Adèle Faucherre*<sup>1</sup>, †*Hamid Moha ou Maati*<sup>1</sup>, *Nathalie Nasr*<sup>1</sup>, *Amélie Pinard*<sup>2</sup>, *Alexis*  
6 *Theron*<sup>2,3</sup>, *Gaëlle Odelin*<sup>2</sup>, *Jean-Pierre Desvignes*<sup>2</sup>, *David Salgado*<sup>2</sup>, *Gwenaëlle Collod-*  
7 *Béroud*<sup>2</sup>, *Jean-François Avierinos*<sup>2,4</sup>, *Guillaume Lebon*<sup>1</sup>, \**Stéphane Zaffran*<sup>2</sup>, \**Chris Jopling*<sup>1</sup>

8  
9 <sup>1</sup> Institut de Génomique Fonctionnelle, Université de Montpellier, CNRS, INSERM  
10 LabEx ICST, Montpellier, France

11 <sup>2</sup>Aix Marseille Univ, INSERM, MMG UMR1251, 13005 Marseille, France.

12 <sup>3</sup>Service de Chirurgie Cardiaque, AP-HM, Hôpital de la Timone, 13005, Marseille, France.

13 <sup>4</sup>Service de Cardiologie, AP-HM, Hôpital de la Timone, 13005, Marseille, France.

14  
15  
16 Corresponding authors-

17 Chris Jopling, PhD, Email: [chris.jopling@igf.cnrs.fr](mailto:chris.jopling@igf.cnrs.fr)

18 Stephane Zaffran PhD, Email: [stephane.zaffran@univ-amu.fr](mailto:stephane.zaffran@univ-amu.fr)

19  
20 † Co-first authors.

21 \*Co-corresponding authors.

26 **Abstract**

27 **Aims-** During embryogenesis, the onset of circulatory blood flow generates a variety of  
28 hemodynamic forces which reciprocally induce changes in cardiovascular development and  
29 performance. It has been known for some time that these forces can be detected by as yet  
30 unknown mechanosensory systems which in turn promote cardiogenic events such as outflow  
31 tract and aortic valve development. PIEZO1 is a mechanosensitive ion channel present in  
32 endothelial cells where it serves to detect hemodynamic forces making it an ideal candidate to  
33 play a role during cardiac development. We sought to determine whether PIEZO1 is required  
34 for outflow tract and aortic valve development.

35

36 **Methods and results-**By analysing heart development in zebrafish we have determined that  
37 *piezol* is expressed in the developing outflow tract where it serves to detect hemodynamic  
38 forces. Consequently, disrupting Piezo1 signalling leads to defective outflow tract and aortic  
39 valve development and indicates this gene may be involved in the etiology of congenital heart  
40 diseases. Based on these findings, we analysed genomic data generated from patients who suffer  
41 from left ventricular outflow tract obstructions (LVOTO) and identified 3 probands who each  
42 harboured potentially pathogenic variants in *PIEZO1*. Subsequent *in vitro* and *in vivo* assays  
43 indicates that these variants behave as dominant negatives leading to an inhibition of normal  
44 PIEZO1 mechanosensory activity. Expressing these dominant negative *PIEZO1* variants in  
45 zebrafish endothelium leads to defective aortic valve development.

46

47 **Conclusion-** These data indicate that the mechanosensitive ion channel *piezol* is required for  
48 OFT and aortic valve development.

49

50

## 51 **Introduction**

52           In many species, the onset of circulation precedes the role it will play later in life as an  
53 oxygen and nutrient delivery system<sup>1</sup>. As the primitive heart initiates circulation, the forces  
54 generated by the blood flow are detected by mechanosensory systems present in the  
55 endothelium which lines both the heart and vasculature<sup>2</sup>. These extracellular forces are  
56 subsequently converted into intracellular signals which can trigger a variety of cellular  
57 responses<sup>3</sup>. Many lines of evidence suggest that the hemodynamic forces generated by the  
58 circulatory system act as epigenetic cues to drive developmental processes such as  
59 cardiogenesis and valvulogenesis forward<sup>4, 5</sup>. Although a number of mechanosensory systems  
60 with the potential to sense circulatory hemodynamics have been identified, our knowledge of  
61 how the endothelium detects mechanical stimuli is far from complete<sup>2, 6</sup>. PIEZO1 is a  
62 mechanosensitive ion channel present in the cell membrane. When the cell membrane is  
63 stretched, this opens the channel and allows an influx of cations<sup>7</sup>. Recently, PIEZO1 has been  
64 shown to confer mechanosensitivity to endothelial cells allowing them to detect hemodynamic  
65 shear stress and subsequently align themselves in the correct orientation during vasculogenesis<sup>8</sup>.  
66 <sup>9</sup>. Furthermore, deleterious mutations in *PIEZO1* are associated with lymphedema in humans  
67 which is caused by defective lymphatic valve development<sup>10</sup>.

68           The outflow tract (OFT) is a transient structure which is extensively remodeled during  
69 development and will give rise to a variety of cardiovascular structures including the aortic and  
70 pulmonary valves. Although it is well established that hemodynamic blood flow plays a role in  
71 OFT development and the formation of the aortic valves<sup>11</sup>, the mechanosensors that detect these  
72 forces have remained elusive. However, because of its role in sensing shear stress in the  
73 vasculature, *PIEZO1* makes a promising candidate for detecting similar forces in the OFT.

74           Here we report that disrupting Piezo1 signalling in zebrafish leads to defective  
75 development of the OFT and aortic valves. Based on these findings we have been able to

76 identify 3 independent predicted pathogenic *PIEZO1* variants in patients with LVOTO.  
77 Furthermore, *in vitro* electrophysiological analysis indicates that all variants are dominant  
78 negatives which significantly inhibit wild type PIEZO1 activity and affect aortic valve  
79 development when expressed in the zebrafish endothelium.

80

81

## 82 **Methods**

### 83 **Zebrafish strains and husbandry.**

84 Zebrafish were maintained under standardized conditions and experiments were conducted in  
85 accordance with local approval (APAFIS#4054-2016021116464098 v5) and the European  
86 Communities council directive 2010/63/EU. Embryos were staged as described<sup>12</sup>. The  
87 *Tg(fli1a:GFP)y1Tg* was provided by the CMR[B] *Centro de Medicina Regenerativa de Barcelona*.  
88 *The double transgenic line Tg(fli1a:GFP)y1;Tg(cmlc2a:RFP)* was generated in house. All larvae  
89 were euthanised by administration of excess anaesthetic (Tricaine).

90

### 91 **Aortic valve imaging**

92 One day prior imaging, larvae were incubated in 0.2  $\mu$ M BODIPY-FL Ceramide (Invitrogen  
93 D3521) in Embryo medium + PTU (0.003% 1-phenyl-2-thiourea). Larvae were then  
94 anesthetized with Tricaine (0.16g/L) and mounted in low melting agarose. Imaging was  
95 performed with a Zeiss LSM710 two-photon microscope coupled to a Ti:sapphire laser  
96 (Spectra-Physics, Santa Clara, CA, USA) and a water immersion 25 $\times$  objective.

97

### 98 **Electrophysiology**

99 All electrophysiological experiments were performed after 2-6 days of culture for transfected  
100 HEK-293T cells seeded at a density of 20 000 cells/35mm dish and after 2-8 hours of culture

101 of freshly dissociated embryonic zebrafish endothelial cells. Dishes were placed on an inverted  
102 microscope (DIAPHOT 300, Nikon). Recordings were performed in inside out or cell attached  
103 configuration for the patch clamp technique. PIEZO1 currents were elicited by a negative  
104 pressure step from 0 to -80mmHg with -10mmHg step increments at -80mV potential.  
105 Stimulation protocols and data acquisition were carried out using a PC (Hewlett Packard) with  
106 commercial software and hardware (pClamp 10.4) (supplemental information).

107

## 108 **Exome sequencing**

109 The exonic sequences were captured with the Agilent Sure Select All Exon v4 kit (Agilent,  
110 Santa Clara, CA, USA) and sequencing was performed on an Illumina HiSeq2000 sequencing  
111 apparatus (Illumina, San Diego, CA, USA). Raw Exome sequencing data were aligned against  
112 the human reference genome hs37decoy5 and duplicated reads were identified using the SNAP  
113 alignment tool version 1.0beta23. For detailed information regarding coverage etc, see  
114 (Suppl.table.2). GATK 3.4 was used to perform local indel realignment, score base recalibration  
115 and variant calling with the Haplotype Caller. Variations were then selected based on quality  
116 criteria using the Variant Filtration module from GATK. Variant annotation (ANNOVAR) and  
117 prioritization was performed with the VarAFT software (<http://varaft.eu>). Prioritization of the  
118 filtered-in variants was based on expression in aortic valve according to RNA-seq expression  
119 data. Patient recruitment was approved by the Comité de Protection des Patients (13.061).

120

## 121 **Results**

### 122 **Identifying the zebrafish endothelial *PIEZO1* ortholog**

123 Previous research has identified a zebrafish *PIEZO1* ortholog that does not appear to be  
124 expressed in endothelial cells<sup>13</sup>. We have subsequently identified a second *PIEZO1* ortholog,  
125 *piezo1b* (Suppl.Fig.S1). At 24 hours post fertilization (hpf), we could detect a weak *piezo1b*

126 signal in the developing heart tube (Suppl.fig.2.A). By 48hpf a strong expression of *piezo1b*  
127 appeared in the AV canal and OFT (Suppl.fig.2.B). By 4 days post fertilization (dpf) we were  
128 able to observe a strong expression of *piezo1b* in the OFT and vasculature (Fig.1.A,B and  
129 suppl.fig.2.C). Furthermore, we were also able to co-localise *piezo1b* with GFP labelled  
130 endothelial cells in the OFT and endocardium and were unable to detect any co-localisation  
131 with GFP labelled myocardium (Fig.1.C-E and suppl.fig.2.D-I). These results indicate that  
132 *piezo1b* is expressed in endothelial cells during zebrafish development, similar to its  
133 mammalian counterpart<sup>9</sup>.

134 We next sought to determine whether Piezo1b is a functional mechanosensitive ion channel in  
135 the developing zebrafish endothelium. To achieve this, we performed electrophysiological  
136 analysis of cultured zebrafish sorted endothelial cells subjected to mechanical stimulation  
137 (Fig.1.F,G). Furthermore, we found that knockdown of *piezo1b* abolishes mechanically induced  
138 currents which was not the case when we targeted *piezo2*<sup>14</sup> its ortholog (Fig.1.F,G). As an  
139 additional control, we performed the same electrophysiological analysis on WT endothelial  
140 cells treated with the PIEZO channel inhibitory peptide GsMTx4<sup>15</sup> and also observed a  
141 reduction in the amplitude of mechanically induced currents (Fig.1.F,G). These data indicate  
142 that Piezo1b is a functional mechanosensitive ion channel present in the endothelial cells of  
143 developing zebrafish embryos.

144

#### 145 ***Piezo1b* is involved in cardiovascular development**

146 Knockdown of *piezo1b* produced a phenotype characterized by defective cardiogenesis and  
147 associated oedema at 3dpf (Fig.2. A-D'). Because Pz1b expression is not restricted to the  
148 endocardium but also appears in vascular endothelial cells, we injected Pz1b-MO1 into  
149 *Tg(fli1a:GFP)y1Tg* embryos in which all endothelial cells express GFP, clearly delineating the  
150 developing vasculature. Overall, vasculogenesis appears largely unaffected and we were unable

151 to detect any noticeable differences in *flila* driven GFP expression (Suppl.fig.S3.S-V).  
152 However we were able to detect a few abnormally branched blood vessels associated with the  
153 intersegmental veins of the trunk in Pz1b *Tg(flila:GFP)y1Tg* morphants, a phenotype which  
154 did not occur in any of the un-injected *Tg(flila:GFP)y1Tg* embryos (Suppl.fig.S3.U,V).  
155 Although we ensured the specificity of the observed phenotype to the knockdown of *piezolb*  
156 by employing two different morpholinos targeting the same gene, we also analysed mRNA  
157 splicing, morpholino synergy and generated a CRISPR/Cas9 *piezolb* knockout  
158 (Suppl.information and suppl.figs.S3 and S4). We next sought to rescue the *piezolb* morphant  
159 phenotype using mouse *piezol* mRNA (mPz1) which is not targeted by the *piezolb* morpholino  
160 (Pz1b-MO1). In this manner, we found that co-injection of Pz1b-MO1 with 20pg of mPz1 RNA  
161 could rescue the cardiac defects observed in *piezolb* morphants (Suppl.fig.S3.C-F). Analysis  
162 of a number of physiological parameters indicates that *piezolb* morphants exhibit a decreased  
163 cardiac output along with blood regurgitation through the AV canal (Fig.2.E-I and  
164 suppl.information and suppl.fig.S5 and movies S1, S2). Taken together these data indicate that  
165 loss of *piezolb* results in defective cardiac development.

166

### 167 ***Piezo1b* is required for OFT development**

168 Because the OFT is directly adjacent to the ventricle, it is most likely subjected to some of the  
169 most extreme hemodynamic forces which in turn could be detected by Piezo1b to subsequently  
170 initiate the further development of this structure. To test this premise we analysed the dynamics  
171 of the OFT in living zebrafish larvae using live confocal microscopic imagery to focus on a  
172 plane which bisected the OFT. At 2dpf (a time point analogous to the images observed in Fig.2.J  
173 and K) we were able to observe the OFT stretch and relax during the cardiac cycle. At the end  
174 of systole, the OFT achieved a maximum peak inside diameter of 16.87 $\mu$ m (+/-0.24 SEM)  
175 (Fig.2.Q and S and movie S3), whereas during diastole the diameter was reduced to 0 $\mu$ m as the

176 OFT relaxed (Fig.2.R and S and movie S3). We also made similar measurements of the dorsal  
177 aorta as a comparison and found that its diameter increased by only 0.72 $\mu$ m (+/-0.20 SEM)  
178 during systole (Fig.2.S and movie S4). This indicates that indeed hemodynamic forces produce  
179 a strong dynamic response in the OFT endothelium which could potentially be detected by  
180 mechanosensors such as Piezo1b.

181 To determine whether Piezo1b is required for OFT development we analysed this structure in  
182 WT and *piezo1b* morphants. At 48hpf, we could not detect any discernible differences between  
183 WT and *piezo1b* morphant embryos (Fig.2.J,K). However, by 72hpf, the WT OFT had  
184 developed into a “pear shaped” structure which was noticeably wider at the interface with the  
185 myocardium when compared to the *piezo1b* morphant OFT (Fig.2.L-P). Furthermore we were  
186 able to rescue this defect by co-injecting mouse *Piezo1* RNA (Suppl.fig.S3.Q,R). Another  
187 prominent feature of OFT development in zebrafish is the strong expression of *elastin* in this  
188 region. Zebrafish possess two *elastin* paralogs, *elastin A (elnA)* and *elastin B (elnB)*. Previous  
189 research indicates that *elnA* is expressed earliest at around 2dpf in the developing jaw cartilage  
190 and OFT. *ElnB* can be detected at 3dpf and becomes predominantly and strongly expressed in  
191 the OFT<sup>16</sup>. We confirmed these results by performing whole mount *in situ* hybridisation (ISH)  
192 using probes specific for either *elnA* or *elnB*. We were unable to detect expression of either  
193 gene in the OFT at 2dpf. However by 3dpf there was a pronounced expression of *elnB* in the  
194 OFT region while *elnA* was also expressed in this region albeit to a lesser extent (Fig.3.A,B).

195 To determine the cellular source of ElnB we performed immunohistochemistry using an anti-  
196 ElnB antibody on *Tg(fli1a:GFP)y1*. Accordingly, we were able to detect ElnB protein being  
197 produced around the OFT, however it did not co-localise with the endothelium and appears  
198 instead to be produced by a population of cells which ensheath the OFT endothelium (Fig.3.C-  
199 E). To determine whether *elnB* expression is reliant on *pz1b*, we analysed its expression in  
200 *piezo1b* morphants. We found that *elnB* expression was severely diminished in the OFT of

201 *piezo1b* morphants when compared to control embryos (Fig.3.F and G.). Furthermore, we found  
202 that co-injection of mouse *Piezo1* mRNA was able to significantly restore *elnB* expression in  
203 the OFT of *piezo1b* morphants (Fig.3.H and I). How *piezo1b* is regulating *elnB* expression is at  
204 present unclear, potentially it could be *via* a intercellular signaling mechanism triggered by  
205 *piezo1b* in the endothelium or *via* a intracellular signaling mechanism triggered by *piezo1b* in  
206 the cells which ensheathe the OFT.

207

### 208 ***Piezo1b* is required for aortic valve development**

209 During cardiac development, the aortic valves will form in the OFT, a process reliant on  
210 hemodynamic forces. Based on this notion we analysed the developing aortic valves to  
211 determine whether *piezo1b* is involved in this process. To achieve this we labelled 7dpf larvae  
212 with BODIPY and imaged them using 2 photon microscopy, a technique which has previously  
213 been employed to analyse the development of the atrioventricular valves in zebrafish<sup>17</sup>. Our  
214 analysis of WT larvae indicates that at this time point two defined leaflets have formed which  
215 function effectively to regulate the flow of blood as it is ejected from the ventricle (Fig.4.A and  
216 Movie.S5). In comparison, the valves in *piezo1b* morphants are highly dysmorphic and appear  
217 to be enlarged and misshapen (Fig.4.B and Movie.S6). A similar aortic valve phenotype is also  
218 apparent in decompensated NMDI treated *piezo1b* KO larvae (Suppl.Fig.S6.). To assess this in  
219 more detail we performed a quantification of the defective valves by dividing the length of  
220 either leaflet by its width (Fig.4.F and suppl.Fig.S6). We observed a significant reduction in the  
221 length/width ratio in *piezo1b* morphants compared to un-injected wildtype larvae indicating that  
222 the aortic valves have failed to develop normally.

223 Previous research in mammals and humans has determined that *NOTCH1* is required for aortic  
224 valve development and mutations in this gene are associated with BAV, a common cause of  
225 left ventricular outflow tract obstruction (LVOTO)<sup>18</sup>. In this regard we next analysed the aortic

226 valves in *notch1b* KO zebrafish larvae. Similar to *piezo1b* morphants, the aortic valves in  
227 *notch1b* mutants are also highly dysmorphic compared to WT controls (Fig.4.C,F and  
228 Movie.S7). The *epidermal growth factor receptor* (EGFR) gene has also been implicated in the  
229 etiology of LVOTO<sup>19</sup>, furthermore previous research in zebrafish has indicated that chemical  
230 inhibition of EGFR using either PKI166 or AG1478 results in defective OFT development<sup>20</sup>.  
231 Based on this we treated zebrafish embryos with either inhibitor for 7 days and again assessed  
232 aortic valve development. As with *piezo1b* morphants and *notch1b* mutants, inhibition of EGFR  
233 results in dysmorphic aortic valves (Fig.4.D,E,F). Taken together these data indicate that loss  
234 of *piezo1b* results in defective aortic valve development and, furthermore, the resulting  
235 phenotype is reminiscent of the valve phenotype caused by disrupting LVOTO associated  
236 genes/proteins in zebrafish. Lastly, based on the phenotypic similarities between *piezo1b*  
237 morphants and larvae in which either NOTCH or EGFR signalling has been disrupted, we  
238 sought to determine whether Piezo1b could in fact be a downstream component of either of  
239 these signalling pathways. To meet this end we performed *in situ* hybridisation for *piezo1b* on  
240 either *notch1b* mutants or EGFR inhibitor treated larvae. In this manner we were unable to  
241 detect any noticeable difference in *piezo1b* expression in either condition and confirmed this  
242 finding by qPCR (Suppl.fig.S7). This indicates that Piezo1b is not a downstream component of  
243 either the NOTCH or EGFR signalling pathways.

244

245

#### 246 **Identification of pathogenic *PIEZO1* variants.**

247 To identify pathogenic mutations in *PIEZO1* we examined whole exome sequence data  
248 generated in-house from 19 patients diagnosed with LVOTO, a spectrum of conditions we  
249 believed encompassed the phenotype we observed in zebrafish. In parallel, we also analysed  
250 whole exome sequence data from 30 LVOTO patients provided by the National Heart, Lung,

251 and Blood Institute (NHLBI) Bench to Bassinet Program: The Pediatric Cardiac Genetics  
252 Consortium (PCGC) dataset (dbGaP accession phs000571.v3.p2.). In this manner, we were able  
253 to identify 3 independent nonsynonymous variants in *PIEZO1*: p.Tyr2022His (c.6064T>C;  
254 p.Y2022H; located in a transmembrane C-terminal domain (in-house analysis)), p.Lys2502Arg  
255 (c.7505A>G; p.K2502R; located in the cytoplasmic C-terminal region of PIEZO1 (in-house  
256 analysis)) and p.Ser217Leu (c. 650C>T; p.S217L; located in N-terminal region (PCGC  
257 analysis)) (Fig.5.A-C). The heterozygous p.Y2022H and p.K2502R variants were subsequently  
258 validated by Sanger sequencing (Fig.5.B,C). Although this was not possible for the p.S217L  
259 variant, we were able to determine that one of the parents also harboured this mutation  
260 indicating that the proband is heterozygous for this variant. According to gnomAD<sup>21</sup>, all 3  
261 variants are considered rare, with minor allele frequencies <1% (Table.1). By comparing  
262 PIEZO1 orthologs in different species it is apparent that Tyr<sub>2022</sub>, Lys<sub>2502</sub> and Ser<sub>217</sub> are  
263 evolutionary conserved amino acids (Fig.5.F). To determine the potential functional  
264 consequences these variants have on PIEZO1, they were analysed using the CADD<sup>22</sup>, Mutation  
265 Taster<sup>23</sup> and UMD Predictor programs<sup>24</sup> (Table.1). In this manner, all 3 variants are predicted  
266 to be pathogenic. Interestingly the diagnostic phenotype which is common to all 3 probands is  
267 bicuspid aortic valve disease (BAV).

268

### 269 **Clinical analysis of patients harboring variants in *PIEZO1*.**

270 The BAV phenotype found in the p.Y2022H and p.K2502R probands was diagnosed by  
271 echocardiography (Fig.5.G-I). The proband carrying the p.Y2022H (c.6064T>C) variant was  
272 diagnosed in childhood with several congenital malformations including a BAV without  
273 ascending aorta aneurysm, a left arm agenesis, a bicornate uterus and a urogenital malformation.  
274 Physical examination revealed an aortic murmur at the third intercostal space. Transthoracic  
275 echocardiography showed a BAV (Fig.5.H and movie S8) with a raphe between the right and

276 the non-coronary leaflets (so called I, R/NC, regarding the Sievers classification) and a mild-  
277 to-moderate aortic regurgitation (Effective regurgitant orifice area = 16mm<sup>2</sup>) due to a prolapse  
278 of the anterior leaflet.

279 The proband carrying the p.K2502R (c.7505A>G) variant was incidentally diagnosed at 13  
280 years old. Family medical history revealed that his mother had a mitral valve prolapse.  
281 However, we have no further information on the mother's genotype. Physical examination  
282 revealed a 3/6 holodiastolic murmur. Transthoracic echocardiography showed a BAV (Fig. 5.I,  
283 and movie S9) with a raphe between the right and the left coronary leaflets (I, R/L, regarding  
284 the Sievers classification) and a moderate aortic regurgitation (Effective regurgitant orifice area  
285 = 20mm<sup>2</sup>) due to a prolapse of the anterior leaflet. There was no dilatation of the ascending  
286 aorta. Left ventricular ejection fraction was 70%.

287 The proband (dbGaP Subject ID-711051) harboring the p.S217L (c. 650C>T) variant was  
288 diagnosed in adolescence (age 17.3 years old) by echocardiography with a BAV R/NC fusion.  
289 Further cardiac analysis revealed no other associated cardiac defects (cardiac situs, systemic  
290 vein, hepatic vein, pulmonary vein, right atrium, atrial septum, left atrium, atrioventricular  
291 junction, tricuspid valve, mitral valve, right ventricle, left ventricle, pulmonary valve, coronary  
292 arteries, pulmonary arteries and aorta are normal). The proband is a caucasian male born in the  
293 United States of America, he stands at 162.2cm tall and weighs 117kg, he presented with no  
294 other extra cardiac abnormalities. His mother and father are caucasian Americans and were 22  
295 and 26 years of age respectively at the birth of the proband. The mother also harbors the same  
296 p.S217L variant. Although the mother has no reported history of heart disease, we have no  
297 information regarding whether or not she has undergone echocardiography to detect BAV (a  
298 limitation of the study recognized by the PCGC). No further information regarding the mother  
299 is available. Although it is very interesting to note that all 3 probands have been diagnosed with

300 BAV it will require a much larger cohort and detailed familial data to determine whether or not  
301 *PIEZO1* is indeed associated with this condition.

302

### 303 **Functional analysis of pathogenic *PIEZO1* variants.**

304 To determine whether the identified variants affected PIEZO1 protein function, we performed  
305 mechano-electrophysiology analysis of HEK-293T cells transfected with either wildtype (WT)  
306 human *PIEZO1* or the p.Y2022H, p.K2502R and p.S217L variants. In this manner we were  
307 able to detect changes in current from HEK cells transfected with wildtype human *PIEZO1*  
308 (Fig.5.A,E). Conversely, cells which had been transfected with either p.Y2022H, p.K2502R or  
309 p.S217L *PIEZO1* variants showed significantly reduced mechano-stimulated currents (Fig.5.B-  
310 E). One explanation for the reduction in *PIEZO1* activity associated with these variants is that  
311 the mutations result in a reduction of cell surface expression. To assess this possibility we  
312 performed immunohistochemistry (IHC) on HEK-293T cells transfected with either wildtype  
313 human *PIEZO1* the p.Y2022H, p.K2502R or p.S217L *PIEZO1* variants. Confocal images of  
314 transfected cells indicates that none of the variants appear to significantly affect the localization  
315 of PIEZO1 to the cell surface when compared to wildtype PIEZO1 (Fig.5.F). To confirm this  
316 observation we measured the fluorescent intensity across the cell membrane. In this manner,  
317 wildtype PIEZO1 and all of the variants show a clear peak of intensity at the cell surface which  
318 drops sharply on the extracellular and intracellular sides when compared to GFP, which is  
319 expressed throughout the cell (Fig.5.G). This shows that aberrant trafficking of PIEZO1 to the  
320 cell surface is not the reason for the observed reduction in activity. These data indicate that the  
321 variants p.Y2022H, p.K2502R and p.S217L have deleterious effects on PIEZO1 protein  
322 function.

323

324 **p.Y2022H, p.K2502R and p.S217L *PIEZO1* variants are dominant negative isoforms.**

325 Because all 3 probands are heterozygous for their respective variants, we next sought to  
326 ascertain whether these variants were dominant negatives. When wildtype human *PIEZO1* was  
327 co-transfected with either p.Y2022H, p.K2502R or p.S217L *PIEZO1* variants, there was a  
328 significant decrease in current amplitude compared to the control (Fig.6.A-E). Taken together  
329 these data indicate that the p.Y2022H, p.K2502R and p.S217L *PIEZO1* variants act as dominant  
330 negatives.

331 Next we sought to determine whether expression of the dominant negative human  
332 *PIEZO1* variants in the zebrafish endothelium could also affect aortic valve development. To  
333 achieve this we generated a transgenic construct using a previously characterised endothelial  
334 specific *fliEP* promoter<sup>25</sup> to drive expression of either WT *PIEZO1* or the variants specifically  
335 in endothelial cells *in vivo* (Suppl.fig.S8.A-G). In this manner we were able to determine that  
336 expressing any of the dominant negative variants (p.Y2022H, p.K2502R or p.S217L) also had  
337 a significant impact on aortic valve development when compared to WT *PIEZO1* endothelial  
338 expression. To assess this in more detail we performed a quantification of the defective valves  
339 by dividing the length of either leaflet by its width (Fig.7.A,B). In this manner we found that  
340 all the variants significantly reduced the overall length/width ratio in both leaflets when  
341 compared to the WT *PIEZO1* expressing larvae. This indicates that expression of either  
342 Y2022H, p.K2502R or p.S217L *PIEZO1* disrupts aortic valve development in zebrafish.

343

## 344 **Discussion**

345 Here we have shown that the mechanosensitive ion channel Piezo1b is required for OFT/aortic  
346 valve development in zebrafish. In particular knockdown of *piezo1b* mRNA leads to a  
347 constricted OFT and dysmorphic aortic valves. We have also identified 3 novel pathogenic  
348 *PIEZO1* variants in patients who suffer from LVOTO. All 3 variants are dominant negative

349 isoforms which when expressed in the developing zebrafish endothelium disrupt aortic valve  
350 development, confirming our results achieved by *piezo1b* knockdown. We believe that this is  
351 the first description of dominant negative PIEZO1 isoforms and future research will be required  
352 to determine whether these variants are indeed associated with LVOTO. However, our data  
353 does highlight a role for Piezo1b in the developing zebrafish OFT and aortic valves where it  
354 serves to detect hemodynamic forces associated with the cardiac cycle and subsequently drive  
355 development forward, which would fit with a role for this gene in the etiology of LVOTO.  
356 Although our data indicate that *piezo1b* is required in the endothelium during aortic valve  
357 development it should also be stressed that other cell types involved in this process, such as  
358 smooth muscle cells (SMC), may also require *piezo1b*. Indeed a recent study by Duchemin *et*  
359 *al*, which corroborates many of our own findings, indicates that *piezo1* expressing SMC play a  
360 significant role in aortic valve development<sup>26</sup>.

361         Despite the differences in cardiac physiology, early OFT development is highly  
362 conserved between mammals and zebrafish, in particular this region will give rise to the aortic  
363 valves. Indeed, elegant studies in avian models have indicated that disrupting hemodynamic  
364 forces, either by increasing or decreasing flow/pressure, significantly disrupts a variety of  
365 cardiac developmental processes including OFT and aortic valve development<sup>27</sup>. Recently, it  
366 has been established that in developing zebrafish larvae the coordinated actions of the  
367 mechanosensitive ion channels TRPV4 and TRPP2 are required to promote *klf2a* expression in  
368 the atrioventricular canal and subsequently drive valve morphogenesis in this region<sup>28</sup>. Our data  
369 indicates that Piezo1 plays a similar role in the developing OFT region. Another gene which  
370 has been implicated in aortic valve development is EGFR due to its association with BAV in  
371 humans<sup>29</sup>. Likewise, *Egfr* KO mice (also known as Wave mice) develop abnormal, functionally  
372 defective aortic valves resulting in regurgitation of blood through this region<sup>30</sup>. Previously it  
373 has been shown that treatment of zebrafish larvae with the EGFR inhibitors PKI166 and

374 AG1478 results in defective OFT development<sup>20</sup>. In agreement with these findings our own  
375 data indicates that Egfr is required for aortic valve development in zebrafish and when this  
376 process is disrupted this results in a defective valve phenotype very similar to that observed in  
377 *piezo1b* morphants. *NOTCH1* is one of the few genes directly linked to BAV in humans<sup>18</sup>. Our  
378 own data indicates that the zebrafish *NOTCH1* ortholog *notch1b* also regulates aortic valve  
379 development. Indeed, zebrafish *notch1b* mutants display dysmorphic valves. Importantly, we  
380 also observed a very similar aortic valve phenotype in *piezo1b* morphant larvae indicating that  
381 this gene is also required for aortic valve development. Although our data indicates that Piezo1b  
382 is not a downstream component of either NOTCH or EGFR signaling pathways future  
383 investigations will be aimed at trying to ascertain whether any synergy exists between these  
384 pathways during aortic valve development. Lastly, all 3 probands have been diagnosed with  
385 bicuspid aortic valve (BAV), however it will require a much larger cohort and detailed familial  
386 data to determine whether or not *PIEZO1* is indeed associated with this condition.

387

### 388 **Funding**

389 This work was supported by INSERM and CNRS. Work in the C.J lab is supported by a grant  
390 from the Fondation Leducq. Work in the C.J lab is supported by a grant from Fondation pour  
391 la Recherche sur le Cerveau “Espoir en tête 2017”. C.J was supported by an INSERM ATIP-  
392 AVENIR grant and a Marie Curie CIG (PCIG12-GA-2012-332772). H.M.M is supported by a  
393 grant from the Association Française contre les Myopathies (AFM-Telethon). A.F was  
394 supported by a Fondation Lefoulon-Delalande postdoctoral fellowship with previous support  
395 provided by a Fondation pour la Recherche Médicale (FRM) postdoctoral fellowship. N.N is  
396 supported by the LabexICST PhD program. A.F, H.M.M, N.N and C.J are members of the  
397 Laboratory of Excellence « Ion Channel Science and Therapeutics » supported by a grant from  
398 the ANR. A.P. received a PhD fellowship from the Association Française du Syndrome de

399 Marfan et Apparentés (AFSMa). Work in the G.L lab is supported by a grant from the ANR  
400 (ANR 17 CE18 0001 06 AT2R TRAAK). Work in S.Z lab is supported by the INSERM and the  
401 Association Française contre les Myopathies (AFM-Telethon). IPAM acknowledges the  
402 France-BioImaging infrastructure supported by the French National Research Agency (ANR-  
403 10-INBS-04, «Investments for the future»), the Fondation pour la Recherche sur le Cerveau  
404 “Espoir en tête 2015”, and Fondation Leducq.

405

#### 406 **Acknowledgements**

407 We would like to acknowledge Dr Matteo Mangoni and Dr Joel Nargeot for their input and  
408 support. We would like to thank Prof Ardem Patapoutian for the kind gift of hPIEZO1-pIRES2-  
409 GFP. We would like to thank Dr Emmanuel Bourinet for the kind gift of mPiezo1. We would  
410 like to thank Dr Yaniv Hintis (Kings College London, UK) and Prof Fred Keeley and Dr Megan  
411 Miao (Hospital for Sick Children, Toronto, CA) for kindly donating the ElnB antibody. We  
412 would also like to acknowledge the Montpellier MGX Genomix platform for their input and  
413 support. Part of this data was generated by the Pediatric Cardiac Genomics Consortium  
414 (PCGC), under the auspices of the National Heart, Lung, and Blood Institute's Bench to  
415 Bassinet Program <<http://www.benchtobassinet.org/>>. The Pediatric Cardiac Genomics  
416 Consortium (PCGC) program is funded by the National Heart, Lung, and Blood Institute,  
417 National Institutes of Health, U.S. Department of Health and Human Services through grants  
418 U01HL098123, U01HL098147, U01HL098153, U01HL098162, U01HL098163, and  
419 U01HL098188. This manuscript was not prepared in collaboration with investigators of the  
420 PCGC, has not been reviewed and/or approved by the PCGC, and does not necessarily reflect  
421 the opinions of the PCGC investigators or the NHLBI. We thank Anthony Pinot from the *in*  
422 *vivo* imaging platform IPAM-Biocampus Montpellier.

423

424 **Conflicts of Interests**

425 None declared

426 **References**

- 427 1. Granados-Riveron JT, Brook JD. The impact of mechanical forces in heart morphogenesis. *Circ*  
428 *Cardiovasc Genet* 2012;**5**:132-142.
- 429 2. Freund JB, Goetz JG, Hill KL, Vermot J. Fluid flows and forces in development: functions,  
430 features and biophysical principles. *Development* 2012;**139**:1229-1245.
- 431 3. Lansman JB, Hallam TJ, Rink TJ. Single stretch-activated ion channels in vascular endothelial  
432 cells as mechanotransducers? *Nature* 1987;**325**:811-813.
- 433 4. Goetz JG, Steed E, Ferreira RR, Roth S, Ramspacher C, Boselli F, Charvin G, Liebling M, Wyart C,  
434 Schwab Y, Vermot J. Endothelial cilia mediate low flow sensing during zebrafish vascular  
435 development. *Cell Rep* 2014;**6**:799-808.
- 436 5. Hove JR, Koster RW, Forouhar AS, Acevedo-Bolton G, Fraser SE, Gharib M. Intracardiac fluid  
437 forces are an essential epigenetic factor for embryonic cardiogenesis. *Nature* 2003;**421**:172-  
438 177.
- 439 6. Busse R, Fleming I. Vascular endothelium and blood flow. *Handb Exp Pharmacol* 2006:43-78.
- 440 7. Coste B, Xiao B, Santos JS, Syeda R, Grandl J, Spencer KS, Kim SE, Schmidt M, Mathur J, Dubin  
441 AE, Montal M, Patapoutian A. Piezo proteins are pore-forming subunits of mechanically  
442 activated channels. *Nature* 2012;**483**:176-181.
- 443 8. Li J, Hou B, Tumova S, Muraki K, Bruns A, Ludlow MJ, Sedo A, Hyman AJ, McKeown L, Young  
444 RS, Yuldasheva NY, Majeed Y, Wilson LA, Rode B, Bailey MA, Kim HR, Fu Z, Carter DA, Bilton J,  
445 Imrie H, Ajuh P, Dear TN, Cubbon RM, Kearney MT, Prasad RK, Evans PC, Ainscough JF, Beech  
446 DJ. Piezo1 integration of vascular architecture with physiological force. *Nature* 2014.
- 447 9. Ranade SS, Qiu Z, Woo SH, Hur SS, Murthy SE, Cahalan SM, Xu J, Mathur J, Bandell M, Coste B,  
448 Li YS, Chien S, Patapoutian A. Piezo1, a mechanically activated ion channel, is required for  
449 vascular development in mice. *Proc Natl Acad Sci U S A* 2014;**111**:10347-10352.
- 450 10. Nonomura K, Lukacs V, Sweet DT, Goddard LM, Kanie A, Whitwam T, Ranade SS, Fujimori T,  
451 Kahn ML, Patapoutian A. Mechanically activated ion channel PIEZO1 is required for lymphatic  
452 valve formation. *Proc Natl Acad Sci U S A* 2018;**115**:12817-12822.
- 453 11. Menon V, Eberth JF, Goodwin RL, Potts JD. Altered Hemodynamics in the Embryonic Heart  
454 Affects Outflow Valve Development. *Journal of cardiovascular development and disease*  
455 2015;**2**:108-124.
- 456 12. Kimmel CB, Ballard WW, Kimmel SR, Ullmann B, Schilling TF. Stages of embryonic development  
457 of the zebrafish. *Developmental dynamics : an official publication of the American Association*  
458 *of Anatomists* 1995;**203**:253-310.
- 459 13. Faucherre A, Kissa K, Nargeot J, Mangoni M, Jopling C. Piezo1 plays a role in erythrocyte  
460 volume homeostasis. *Haematologica* 2013.
- 461 14. Faucherre A, Nargeot J, Mangoni ME, Jopling C. piezo2b regulates vertebrate light touch  
462 response. *J Neurosci* 2013;**33**:17089-17094.
- 463 15. Bae C, Sachs F, Gottlieb PA. The mechanosensitive ion channel Piezo1 is inhibited by the  
464 peptide GsMTx4. *Biochemistry* 2011;**50**:6295-6300.
- 465 16. Miao M, Bruce AE, Bhanji T, Davis EC, Keeley FW. Differential expression of two tropoelastin  
466 genes in zebrafish. *Matrix biology : journal of the International Society for Matrix Biology*  
467 2007;**26**:115-124.
- 468 17. Vermot J, Forouhar AS, Liebling M, Wu D, Plummer D, Gharib M, Fraser SE. Reversing blood  
469 flows act through klf2a to ensure normal valvulogenesis in the developing heart. *PLoS Biol*  
470 2009;**7**:e1000246.

- 471 18. Garg V, Muth AN, Ransom JF, Schluterman MK, Barnes R, King IN, Grossfeld PD, Srivastava D.  
472 Mutations in NOTCH1 cause aortic valve disease. *Nature* 2005;**437**:270-274.
- 473 19. Giusti B, Sticchi E, De Cario R, Magi A, Nistri S, Pepe G. Genetic Bases of Bicuspid Aortic Valve:  
474 The Contribution of Traditional and High-Throughput Sequencing Approaches on Research and  
475 Diagnosis. *Frontiers in physiology* 2017;**8**:612.
- 476 20. Goishi K, Lee P, Davidson AJ, Nishi E, Zon LI, Klagsbrun M. Inhibition of zebrafish epidermal  
477 growth factor receptor activity results in cardiovascular defects. *Mechanisms of development*  
478 2003;**120**:811-822.
- 479 21. Lek M, Karczewski KJ, Minikel EV, Samocha KE, Banks E, Fennell T, O'Donnell-Luria AH, Ware  
480 JS, Hill AJ, Cummings BB, Tukiainen T, Birnbaum DP, Kosmicki JA, Duncan LE, Estrada K, Zhao F,  
481 Zou J, Pierce-Hoffman E, Berghout J, Cooper DN, Deflaux N, DePristo M, Do R, Flannick J,  
482 Fromer M, Gauthier L, Goldstein J, Gupta N, Howrigan D, Kiezun A, Kurki MI, Moonshine AL,  
483 Natarajan P, Orozco L, Peloso GM, Poplin R, Rivas MA, Ruano-Rubio V, Rose SA, Ruderfer DM,  
484 Shakir K, Stenson PD, Stevens C, Thomas BP, Tiao G, Tusie-Luna MT, Weisburd B, Won HH, Yu  
485 D, Altshuler DM, Ardissino D, Boehnke M, Danesh J, Donnelly S, Elosua R, Florez JC, Gabriel SB,  
486 Getz G, Glatt SJ, Hultman CM, Kathiresan S, Laakso M, McCarroll S, McCarthy MI, McGovern D,  
487 McPherson R, Neale BM, Palotie A, Purcell SM, Saleheen D, Scharf JM, Sklar P, Sullivan PF,  
488 Tuomilehto J, Tsuang MT, Watkins HC, Wilson JG, Daly MJ, MacArthur DG, Exome Aggregation  
489 C. Analysis of protein-coding genetic variation in 60,706 humans. *Nature* 2016;**536**:285-291.
- 490 22. Kircher M, Witten DM, Jain P, O'Roak BJ, Cooper GM, Shendure J. A general framework for  
491 estimating the relative pathogenicity of human genetic variants. *Nature genetics* 2014;**46**:310-  
492 315.
- 493 23. Schwarz JM, Cooper DN, Schuelke M, Seelow D. MutationTaster2: mutation prediction for the  
494 deep-sequencing age. *Nature methods* 2014;**11**:361-362.
- 495 24. Salgado D, Desvignes JP, Rai G, Blanchard A, Miltgen M, Pinard A, Levy N, Collod-Beroud G,  
496 Beroud C. UMD-Predictor: A High-Throughput Sequencing Compliant System for Pathogenicity  
497 Prediction of any Human cDNA Substitution. *Human mutation* 2016;**37**:439-446.
- 498 25. Villefranc JA, Amigo J, Lawson ND. Gateway compatible vectors for analysis of gene function  
499 in the zebrafish. *Developmental dynamics : an official publication of the American Association*  
500 *of Anatomists* 2007;**236**:3077-3087.
- 501 26. Duchemin AL, Vignes H, Vermot J. Mechanically activated piezo channels modulate outflow  
502 tract valve development through the Yap1 and Klf2-Notch signaling axis. *eLife* 2019;**8**.
- 503 27. Poelmann RE, Gittenberger-de Groot AC. Hemodynamics in Cardiac Development. *Journal of*  
504 *cardiovascular development and disease* 2018;**5**.
- 505 28. Heckel E, Boselli F, Roth S, Krudewig A, Belting HG, Charvin G, Vermot J. Oscillatory Flow  
506 Modulates Mechanosensitive klf2a Expression through trpv4 and trpp2 during Heart Valve  
507 Development. *Current biology : CB* 2015;**25**:1354-1361.
- 508 29. Dargis N, Lamontagne M, Gaudreault N, Sbarra L, Henry C, Pibarot P, Mathieu P, Bosse Y.  
509 Identification of Gender-Specific Genetic Variants in Patients With Bicuspid Aortic Valve. *The*  
510 *American journal of cardiology* 2016;**117**:420-426.
- 511 30. Hajj GP, Chu Y, Lund DD, Magida JA, Funk ND, Brooks RM, Baumbach GL, Zimmerman KA, Davis  
512 MK, El Accaoui RN, Hameed T, Doshi H, Chen B, Leinwand LA, Song LS, Heistad DD, Weiss RM.  
513 Spontaneous Aortic Regurgitation and Valvular Cardiomyopathy in Mice. *Arterioscler Thromb*  
514 *Vasc Biol* 2015;**35**:1653-1662.
- 515 31. Zhao Q, Zhou H, Chi S, Wang Y, Wang J, Geng J, Wu K, Liu W, Zhang T, Dong MQ, Wang J, Li X,  
516 Xiao B. Structure and mechanogating mechanism of the Piezo1 channel. *Nature* 2018;**554**:487-  
517 492.

## 518 Figure legends

519 **Figure.1. Identifying the zebrafish endothelial *PIEZO1* ortholog.**

520 (A,B) ISH using an antisense *piezo1b* probe. *piezo1b* expression can be detected in the OFT of  
521 zebrafish larvae (yellow arrowhead) at 4dpf. (C-E) Double fluorescent ISH using antisense  
522 GFP (C) and antisense *piezo1b* (D) probes, merged image (E) indicates endothelial GFP and  
523 *piezo1b* co-localise in the OFT endothelium at 4dpf in *Tg(fli1a:GFP)y1* embryos. (F,G)  
524 Electrophysiological recordings of mechanosensitive currents from embryonic endothelial  
525 cells. Currents were recorded via patch clamp using and inside out configuration by application  
526 of negative pressures from 0 to -80mmHg with -10mmHg step increments at -80mV potential.  
527 (F) Typical current traces recorded from cells isolated from control, *piezo1b* MO1, Pz2 MO  
528 injected embryos and cell treated with GsMTx4 *via* the patch clamp pipette. The pressure  
529 stimulation protocol is shown in inset. (G) Corresponding pressure/current curves showing the  
530 activation of the current from control, Pz1b-MO1, Pz2-MO cells and GsMTx4 treated cells (\*  
531  $p < 0,05$ , \*\*  $p < 0.01$ , student's t-test). The red rectangle shows the value of the current amplitude  
532 for the three test conditions at -50 mmHg step stimulation. Scale bars: (A,B) 100 $\mu$ m (E) 10 $\mu$ m.  
533

534 **Figure.2. *Piezo1b* is involved in cardiovascular development.**

535 (A) Un-injected 72hpf zebrafish embryo, (A') the same embryo at higher magnification. (C) A  
536 72hpf *piezo1b* morphant displaying pericardial oedema and defective cardiac looping (black  
537 arrowhead), (C') the same embryo at higher magnification. (n=48/50). (B,B',D,D') ISH using  
538 an antisense *cmhc2a* probe on (B) 72hpf un-injected zebrafish embryos, (B') the same embryo  
539 at higher magnification, the yellow dashed line above the ventricle (v) and atrium (a) is an  
540 indicator for the degree of cardiac looping. (D) 72hpf *piezo1b* morphant embryo, (D') the same  
541 embryo at higher magnification, note the yellow dashed line is no longer horizontal indicating  
542 a defect in cardiac looping (n=48/50). (E) Graph depicting the average heart rate in beats per  
543 minute (BPM) of WT (n=8) and Pz1b morphants (n=8). (F) Graph depicting the average blood  
544 flow rate in nano litres per second (nL/sec) of WT (n=8) and Pz1b morphants (n=8). (G) Graph

545 depicting the average minimum/maximum blood flow rate in nano litres per second (nL/sec) of  
546 WT (n=8) and Pz1b morphants (n=8). (H) Graph depicting the average stroke volume in nano  
547 litres per heart beat (nL/beat) of WT (n=8) and *piezo1b* morphants (n=8). (I) Graph depicting  
548 the average ventricular contractile distance in micro metres ( $\mu\text{M}$ ) of WT (n=5) and Pz1b  
549 morphants (n=5). (J-M) Maximal projections of 48hpf (J,K) and 72hpf (L-M)  
550 *Tg(fli1a:GFP)y1;Tg(cmlc2:RFP)* OFT from WT (J,L) and *piezo1b* morphants (K,M). Yellow  
551 dashed lines delineate the OFT position at 48hpf (J,K). (N,O) Maximal projections of a 72hpf  
552 *Tg(fli1a:GFP)y1* OFT from WT (N) and *piezo1b* morphants (O). The white line indicates the  
553 width of the OFT immediately adjacent to the myocardium. (P) Graph showing the average size  
554 of the OFT of WT and *piezo1b* morphants (n wt=7, n Pz1bMO1=11). (Q) A still image taken  
555 from a resonance laser z-stack movie of a live 48hpf *Tg(fli1a:GFP)y1* zebrafish larvae's OFT  
556 at the end of systole, the yellow dashed lines delineate the edges of the OFT endothelial vascular  
557 walls. The white double headed arrow indicates the OFT inside diameter during systole. (R) A  
558 still image taken from a resonance laser z-stack movie of a live 48hpf *Tg(fli1a:GFP)y1*  
559 zebrafish larvae's OFT during diastole, the yellow dashed lines delineate the edges of the OFT  
560 endothelial vascular walls which are in contact with one another. (S) Graph showing the  
561 difference between OFT and aorta inside diameters between diastole and systole (n=4; 3  
562 contractions for each). All graphs (\* p<0,05, \*\* p<0.01, student's t-test), Scale bars (A-B')  
563 100 $\mu\text{m}$  (J-O and Q,R) 10 $\mu\text{m}$ .

564

565 **Figure.3. Elastin expression in the OFT of zebrafish is dependent on *Piezo1b*.**

566 (A,B) *In situ* hybridization against *elnA* (A) and *elnB* (B) on 3 dpf embryos. (C-E) Single z-  
567 stack confocal images of the OFT following an immunostaining using an anti-ElnB antibody  
568 (C, red) on 3 dpf *Tg(fli1a:GFP)y1* embryos (D, green). The merged image (E) indicates that  
569 the cells producing ElnB are not endothelial which are producing GFP. (F,G) ) *In situ*

570 hybridization against *elnB* in 3 dpf WT (F) and *piezo1b* (G) morphants. (H) *In situ* hybridization  
571 using an antisense *elnB* probe on *piezo1b* morphant embryos co-injected with mouse *Piezo1*  
572 mRNA. Embryos were sorted according to the intensity of *elnB* expression. (I) Percentage of  
573 embryos showing the *elnB* expression levels depicted in (M) in WT, Pz1bMO1 injected or  
574 Pz1bMO1 + m*Piezo1* RNA injected embryos.

575

576

577 **Figure.4. *Piezo1b* is required for aortic valve development.**

578 2 photon images of aortic valves in 7dpf zebrafish larvae labelled with BODIPY. (A)  
579 Representative image of the aortic valves in a WT larvae, valves are outlined with a dashed  
580 white line (n=8). (B) A *piezo1b* morphant (n=6). (C) A *notch1b* mutant (n=11). (D) A AG1478  
581 treated larvae (n=6). (E) A PKI166 treated larvae (n=6). Graph depicting the length to width  
582 ratio for the left and right valve leaflets measured in 7dpf WT larvae, Pz1b morphants, *notch1b*  
583 KO larvae or larvae treated with either AG1478 or PKI166. Error bars indicate SD, ANOVA  
584 and Dunnett's multiple comparisons test  $P < 0.01$  (all samples), student's unpaired homoscedastic  
585 two tailed t-test  $**P < 0.01$ . Scale bars-20 $\mu$ m.

586

587 **Figure.5. Identification of pathogenic variants in *PIEZO1*.**

588 (A) Schematic representation of human PIEZO1 protein, the position of each variant is  
589 indicated by a red dot (adapted from *Zhao et al*<sup>31</sup>). (B,C) Cartoon representation of the mouse  
590 mechanosensitive Piezo1 channel 3D Model (PDB 5Z10). The corresponding residues K2502  
591 (Magenta) and Y2022 (Green) identified in this study as subject to genetic variability are  
592 represented as spheres. (D,E) Sequence chromatographs showing heterozygous variants  
593 c.6064T>C (p.Y2022H; B) and c.7505A>G (p.K2502R; C) in genomic DNA taken from the  
594 affected LVOTO patients. (F) Protein alignments for all 3 variants. Note the strong evolutionary

595 conservation for Tyr2022, Lys2502 and Ser217 residues. **(G-I)** Representative echocardiogram  
596 of the aortic valve from an unaffected individual **(G)** and the BAV patients carrying out the  
597 c.6064T>C; p.Y2022H variant **(H)** and c.7505A>G; p.K2502R variant **(I)**. Note the 3 valve  
598 leaflets in the unaffected individual **(G)** compared to the 2 leaflets in the BAV patients **(H** and  
599 **I)**.

600

601 **Figure.6. Functional analysis of pathogenic *PIEZO1* variants.**

602 Electrophysiological recordings of mechanosensitive currents from all 3 *PIEZO1* variants.  
603 Typical current traces recorded from HEK cells transfected with either wildtype (WT) human  
604 *PIEZO1* (hPz1) **(A)**, human *PIEZO1* c.6064T>C (p.Y2022H) variant **(B)**, human *PIEZO1*  
605 c.7075A>G (p.K2502R) **(C)** variant or human *PIEZO1* c.650C>T (p.S217L) variant **(D)**.  
606 Currents were recorded *via* patch clamp using a cell attached configuration by application of  
607 negative pressures from 0 to -80mmHg with -10mmHg step increments at -80mV potential. **(E)**  
608 Corresponding pressure/current curves showing the activation of the current from wildtype  
609 hPz1, p.Y2022H, p.K2502R and p.S217L (\* p<0,05, \*\* p<0.01, \*\*\* p<0.001 student's t-test).  
610 **(F)** Immunohistochemistry using an anti *PIEZO1* antibody on HEK 293T cells transfected with  
611 either empty vector (pIRES2-GFP), wildtype human *PIEZO1* (wt-hPz1), human *PIEZO1*  
612 c.6064T>C (p.Y2022H) variant (Y2022H-hPz1), human *PIEZO1* c.7075A>G (p.K2502R)  
613 variant (K2502R-hPz1) or human *PIEZO1* c.650C>T (p.S217L) variant (S217L-hPz1). **(G)**  
614 Cell surface immunofluorescent analysis. Fluorescent intensity was measured in ImageJ by  
615 drawing a line through the cell membrane (yellow bar). Graphs plotting the fluorescent intensity  
616 at the cell surface for WT and variant *PIEZO1*. In all cases there is a clear peak of RFP  
617 fluorescent intensity which tapers off on either side of the cell membrane. The control GFP  
618 signal is continuous. Scale bars **(F)** 10µm.

619

620 **Figure.7. The *PIEZO1* variants are dominant negatives**

621 Electrophysiological recordings of mechanosensitive currents from co-transfection of 3  
622 *PIEZO1* variants with wildtype human *PIEZO1*. Typical current traces recorded from HEK  
623 cells co-transfected with either wildtype human *PIEZO1* (hPz1) and empty pIRES2-GFP (**A**),  
624 wildtype human *PIEZO1* (hPz1) and human *PIEZO1* c.6064T>C (p.Y2022H) variant (**B**),  
625 wildtype human *PIEZO1* (hPz1) and human *PIEZO1* c.7075A>G (p.K2502R) variant (**C**) or  
626 wildtype human *PIEZO1* (hPz1) and human *PIEZO1* c.650C>T (p.S217L) (**D**). Currents were  
627 recorded *via* patch clamp using a cell attached configuration by application of negative  
628 pressures from 0 to -80mmHg with -10mmHg step increments at -80mV potential. (**E**)  
629 Corresponding pressure/current curves showing the activation of the current from wildtype  
630 hPz1/empty pIRES2-GFP, wildtype hPz1/p.Y2022H, wildtype hPz1/p.K2502R and wildtype  
631 hPz1/p.S217L (\* p<0,05, \*\* p<0.01, \*\*\* p<0.001 student's t-test).

632

633 **Figure.8. Expression of *PIEZO1* variants *in vivo* disrupts aortic valve development**

634 (**A**) Representative images of aortic valve leaflet quantification in a 7dpf larvae expressing  
635 either WT human *PIEZO1* (hPZ1-wt) or the Y2022H variant of human *PIEZO1* (hPZ1-  
636 Y2022H), ratios were calculated by measuring the length of the leaflet from the lower edge to  
637 the tip, the width was measured at a point halfway along the length (yellow lines). (**B**) Graph  
638 depicting the length to width ratio for the left and right valve leaflets measured in 7dpf larvae  
639 expressing either WT (n=8), K2502R (n=11), Y2022H(n=10) or S217L (n=10) human *PIEZO1*.  
640 Error bars indicate SEM, ANOVA and Dunnet's multiple comparisons test P<0.01(all  
641 samples), student's unpaired homoscedastic two tailed t-test \*\*P<0.01. Scale bars-20µm.

642

## 1 **Supplemental information**

### 2 **Morpholinos**

3 The sequences of the injected MOs are the following:

4 Pz1b MO1: 5'-TCTGTTGCTGGATTCTGTGAATCAT-3'-5ng

5 Pz1b MO2: 5'-ACCCATGATGCTGCAACACACACAC-3'-4ng

6 *tnnt2* MO : 5'-CATGTTTGCTCTGATCTGACACGCA3' -3ng

7 The amount of morpholino used in all experiments is given in nanograms (ng), excluding the suboptimal  
8 experiments where the amounts are indicated in the figure (suppl.fig.S3.K-P).

### 9 **DNA microinjection**

10 The *fli1ep:hPIEZO1* constructs were generated using the Tol2 kit[1]. 478 p5E*fli1ep* was a gift  
11 from Nathan Lawson (Addgene plasmid # 31160 ; <http://n2t.net/addgene:31160> ;  
12 RRID:Addgene\_31160). Wildtype variant *hPIEZO1* were subcloned from pIRES2-GFP into  
13 pME-MCS by restriction digestion and ligation. 5' capped sense RNAs were synthesized using  
14 a construct encoding the transposase and the mMessage mMachine kit (Ambion). 20 pg of the  
15 *Fli1ep:hPiezo1* DNA construct and 20 pg of the transposase sRNA were simultaneously  
16 injected into embryos at the one cell stage.

### 17 **Morpholino and CRISPR/Cas9 control experiments**

18 The Pz1b MO1 and MO2 were designed to block the post-transcriptional splicing of the Pz1b.  
19 As with Pz1b MO1 (Suppl.fig.S3.A,B), we also confirmed that splicing had been disrupted by  
20 performing RT-PCR on Pz1b MO2 morphants (Suppl.fig.S3.I,J). To further ensure that the  
21 observed phenotype is due to specific knockdown of Pz1b, we co-injected suboptimal  
22 concentrations of both Pz1b MO1 and Pz1b MO2. Subsequent *in situ* hybridization with a  
23 *cmlc2a* probe reveals that injection of either morpholino at suboptimal concentrations alone  
24 does not affect heart development (Suppl.fig.S3.K-N). However, co-injection of both  
25 morpholinos at these concentrations results in the same defective cardiac looping phenotype

26 observed at optimal concentrations of either morpholino (Suppl.fig.S3.O,P). Lastly, we also  
27 endeavoured to knockout (KO) Pz1b by employing a CRISPR/Cas9 strategy. To achieve this,  
28 we designed a gRNA which targeted exon 11 of Pz1b. In this manner we were able to generate  
29 a mutant zebrafish line harbouring a 13bp substitution at position 1435 to 1437 in Pz1b resulting  
30 in a frameshift and premature stop codon after 609 amino acids. This line was designated  
31 *piezo1b<sup>mmr5</sup>*. Unfortunately, homozygous *piezo1b<sup>mmr5/mmr5</sup>* embryos did not display any  
32 discernible phenotype. A recent report has indicated that KO of the other *piezo1* zebrafish  
33 paralogue *piezo1a* also does not produce any discernible phenotype [2]. Although it is possible  
34 that zebrafish do not require *piezo1* at all for development, based on the drastic consequences  
35 observed in mammals and humans when *piezo1* is KO or mutated, this seems unlikely [3-5].  
36 We reasoned that the most likely explanation for the lack of phenotype was due to  
37 compensation, as has been reported in other zebrafish KO lines where the expected phenotype  
38 was not observed[6]. To assess this possibility we followed the recently developed morpholino  
39 guidelines[7] and injected the Pz1b morpholino into embryos from an incross of the  
40 *piezo1b<sup>mmr5/mmr5</sup>* line. If compensation has occurred, we should expect that the Pz1b morpholino  
41 would have little effect in homozygous *piezo1b<sup>mmr5/mmr5</sup>* embryos. Indeed, we were able to  
42 observe an obvious oedema and defective cardiac looping in wildtype *piezo1b* morphant  
43 embryos (the embryos were produced by incrossing a *piezo1b<sup>+/+</sup>* line which was established in  
44 parallel to the KO line to maintain the same genetic background), however this defect was  
45 absent in *piezo1b<sup>mmr5/mmr5</sup>* morphants (Suppl.fig.S4.A-C). This indicates that in *piezo1b<sup>mmr5/mmr5</sup>*  
46 zebrafish embryos, *piezo1b* is compensated and thus the Pz1b morpholino has little effect. This  
47 result also confirms that the phenotype we observe in *piezo1b* morphants is specific to  
48 knockdown of Pz1b and is not due to off target effects. To determine whether *piezo1a* could be  
49 compensating for the loss of *piezo1b* we performed qPCR for *piezo1a* on *piezo1b<sup>mmr5/mmr5</sup>*

50 mutants. However we could not detect any significant upregulation in the expression of *piezo1a*  
51 indicating that this gene does not compensate for loss of *piezo1b* (Suppl.Fig.S4.D.).

52 More recently El-Brolosy *et al* have shown that the compensatory mechanism is triggered by  
53 the degradation of the mutant mRNA transcript[8]. Indeed, inhibition of nonsense mediated  
54 decay with NMDI effectively blocks the compensatory effects observed in mutant zebrafish.  
55 We adopted a similar strategy and treated homozygous *piezo1b<sup>mmr5/mmr5</sup>* embryos with NMDI.  
56 In comparison to their wildtype siblings, NMDI treated homozygous *piezo1b<sup>mmr5/mmr5</sup>* embryos  
57 developed a similar cardiac phenotype to that observed in *piezo1b* morphants (Suppl.Fig.6.A.).  
58 Furthermore, these larvae also displayed defective aortic valves which were similar to those  
59 observed in *piezo1b* morphants (Suppl.Fig.S6.B-D.). These data strongly indicate that genetic  
60 compensation has occurred in homozygous *piezo1b<sup>mmr5/mmr5</sup>* embryos but more importantly,  
61 when compensation is inhibited with NMDI, *piezo1b<sup>mmr5/mmr5</sup>* embryos develop defective aortic  
62 valves indicating that *piezo1b* is required for aortic valve development.

63

#### 64 **Zebrafish cardiac performance analysis**

65 The heart is at the centre of the circulatory system and consequently any reduction in its  
66 performance will have wide ranging consequences. Using the  $\mu$ ZebraLab™ system from  
67 ViewPoint [9], we were able to determine that *piezo1b* morphant embryos had a significantly  
68 lower heart rate (160.4bpm +/-3.4SEM) than WT embryos (187.5bpm +/- 0.65SEM) (Fig.2.E).  
69 To investigate this phenotype further, we next analysed a number of blood flow parameters  
70 using the ViewPoint ZebraBlood™ system [9]. In this manner we were able to determine that  
71 the mean blood flow in *piezo1b* morphants was significantly lower than that of un-injected  
72 controls (Fig.2.F). Further analysis of *piezo1b* morphants indicates that the maximal blood flow  
73 (corresponding to cardiac systole) is also markedly reduced when compared to the control  
74 embryos (Fig.2.G). Similarly, the average stroke volume is also significantly lower in the

75 *piezo1b* morphants when compared to un-injected controls (Fig.2.H). The reduced blood flow  
76 rate associated with systole could also be an indicator that cardiac contractility is compromised  
77 in *piezo1b* morphants. To test this we made high-speed video recordings of either wildtype un-  
78 injected embryos or *piezo1b* morphants. Subsequent frame by frame analysis allowed us to  
79 measure the distance that the ventricular wall contracts during a cardiac cycle (Suppl.fig.S5,B).  
80 In this manner, we found that ventricular contraction in *piezo1b* morphants was increased  
81 resulting in a reduced end systolic volume (ESV) (Fig.2.I). Furthermore, we were also able to  
82 observe blood regurgitation occurring between the atrium and ventricle at the end of systole  
83 (movies S1 and S2). Taken together, the decreased ESV and cardiac output observed in *piezo1b*  
84 morphants suggests the presence of OFT stenosis.

85

#### 86 **Zebrafish strains and husbandry.**

87 Zebrafish were maintained under standardized conditions and experiments were conducted in  
88 accordance with local approval (APAFIS#4054-2016021116464098 v5) and the European  
89 Communities council directive 2010/63/EU. Embryos were staged as described [10]. The  
90 *Tg(fli1a:GFP)y1Tg* was provided by the CMR[B] *Centro de Medicina Regenerativa de*  
91 *Barcelona*. The double transgenic line *Tg(fli1a:GFP)y1;Tg(cmlc2a:RFP)* was generated in  
92 house. All larvae were euthanised by administration of excess anaesthetic (Tricaine).

93

#### 94 **Morpholinos and injections**

95 Morpholino oligonucleotides (MOs) were obtained from Gene Tools (Philomath, OR, USA)  
96 and injected into one-cell stage embryos. The Pz1b MO1 and MO2 target the intron 7/exon 8  
97 and the last exon/intron splice site of *piezo1b* (GenBank: KT428876.1) respectively  
98 (supplemental information).

99

100

101

102 **Embryonic zebrafish endothelial primary cell culture.**

103 3dpf *Tg(fli1a:GFP)y1* embryos were placed in a microtube and pipetted up and down 10 times  
104 to remove the yolk sac. Digestion was performed in digestion buffer (2.5mg/mL trypsin, 1mM  
105 EDTA, 0.16mg/mL tricaine in PBS) in the incubator (28°C) and monitored every 10 minutes  
106 and pipetted up and down to dissociate cells mechanically. The reaction was stopped by adding  
107 a same volume of 10% FBS, 2mM CaCl<sub>2</sub>. Cells were pelleted by centrifugation 3 min 3000rpm,  
108 washed with culture medium (L-15, 5% FBS, 1% penicillin/streptavidin) and re-suspended in  
109 culture medium. Cells were plated in a 35mm Petri dish (5 embryos/2mL/per dish) and placed  
110 in an atmosphere of 95% air/5% CO<sub>2</sub> at 30 °C for a minimum 2 hours prior to patch clamp  
111 experiments.

112

113 **Cell surface quantification**

114 For membrane expression quantification of the WT and variant PIEZO1, fluorescence intensity  
115 (grey value) was measured across a line from the outside to the inside of the cell for GFP and  
116 RFP using ImageJ.

117

118 **PIEZO1 3D structure**

119 Residues K2528 (Magenta) and Y2038 (Green) identified in this study as subject to genetic  
120 variability are represented as spheres. Images were produced using PyMOL™ Molecular  
121 Graphics System, Version 1.8.6.0.

122

123 **CRISPR/Cas9**

124 *Piezo1b* target sequences were identified using ZiFiT online software [11]. The *piezo1b* gRNA  
125 was synthesised from a DNA string template from Invitrogen using the Megashortscript T7 kit  
126 (Ambion) and purified by phenol/chloroform extraction. 150pg of *piezo1b* gRNA was co-  
127 injected with nls-Cas9 protein (N.E.B). Embryos were bred to adulthood and initially screened  
128 for mutations in *piezo1b* using a previously described T7 assay [12]. The founder of the  
129 *piezo1b<sup>mmr5</sup>* mutant line was verified by Sanger sequencing and outcrossed to AB wildtype. F1  
130 *piezo1b<sup>mmr5/+</sup>* adults were identified using the T7 assay and verified by Sanger sequencing.

131

### 132 **PKI166 and AG478 treatments**

133 PKI166 AND AG1478 treatments were performed as described [13].

134

### 135 **Electrophysiology**

136 Each current was evaluated using an Axiopatch 200B amplifier (Axon Instrument, USA), low-  
137 pass filtered at 3kHz and digitized at 2kHz using a 12-bit analog-to-digital digidata converter  
138 (1440A series, Axon CNS, Molecular devices, USA). Results are expressed as mean  $\pm$  standard  
139 error of the mean (SEM). Patch clamp pipettes were pulled using vertical puller (PC-10,  
140 Narishige) from borosilicate glass capillaries and had a resistance 1.2-2M $\Omega$  for the inside out  
141 currents. For the whole cell attached currents, the bath solution contained (in mM) 155 KCl, 3  
142 MgCl<sub>2</sub>, 5 EGTA and 10 HEPES adjusted to pH7.2 with KOH. The pipette solution contained  
143 (in mM) 150 NaCl, 5 KCl, 2 CaCl<sub>2</sub>, and 10 HEPES adjusted to pH7.4 with NaOH.

144

### 145 ***In situ* hybridisation**

146 The *piezo1b* probe was generated by cloning a 2kb fragment from a 3dpf zebrafish cDNA  
147 library into pGEMT. The *cmlc2a* probe was generated from pBSK *cmlc2a* containing the full

148 length *cmlc2a* gene. The *elnA* and *elnB* probes were generated by cloning a 1kb fragment from  
149 a 3dpf zebrafish cDNA library into pGEMT.

150

### 151 **Immunohistochemistry**

152 Transfected cells were fixed in 4% PFA for 20min and blocked with PBS, 2mg/mL BSA, 2%  
153 lamb serum for 45min at room temperature. Cells were then incubated in the same solution  
154 with primary rabbit anti-Piezo1 antibody (Proteintech 15939-1-AP, 1/100) for 3h followed by  
155 donkey Alexa Fluor 594-anti rabbit (Jackson ImmunoResearch Laboratories, 1/200) 2h at room  
156 temperature. For whole mount immunohistochemistry, embryos were fixed overnight at 4°C in  
157 a solution of 4% paraformaldehyde in PBS. After fixation, samples were washed in PBS with  
158 0.1% Tween-20 (PBST), permeabilized with acetone for 6 minutes at -20°C and blocked at  
159 room temperature with 10% bovine serum albumin in PBST. Primary antibody incubation was  
160 conducted overnight at 4°C in blocking buffer with the anti-ELNB antibody at a 1:250 dilution  
161 . Secondary-antibody incubation was conducted for 3 hours at room temperature in PBST with  
162 a Cy3 anti-rabbit (Jackson Labs) at a 1:500 dilution.

163

164

### 165 **RT-PCR analysis**

166 30hpf embryos non-injected or injected with 5ng of *piezo1b* MO1 or with 5 or 10ng of *piezo1b*  
167 MO2 were collected and RNA was isolated with TRIzol® Reagent. RT-PCR was performed  
168 on 1µg of RNA using oligo-dT primers and amplification PCR was performed using *piezo1b*  
169 specific primers

170 The sequences of the *piezo1b* specific primers are the following:

171 For (MO1): 5'-GTTTTGATCGTAACGTCAAA-3'

172 Rev (MO1): 5'-TCAGTTGTTTGTGTCTCTTT-3'

173 For (MO2): 5'-ACGGAGTCTATAAGAGCATC-3'

174 Rev (MO2): 5'-TCATTTGTTTTTCTCTCGCG-3'

175

### 176 **Cardiovascular parameters analysis**

177 To determine the cardiovascular parameters, we utilized  $\mu$ ZebraLab™ software from  
178 ViewPoint which has been developed specifically for this purpose. All experiments were  
179 performed as described previously [9]. To determine the mean blood flow, the average of the  
180 blood flow values was calculated from a 10 second time frame (1,300 frames). For the  
181 maximum and minimum blood flow, averages of highest and lowest peak values were  
182 calculated during 20 heartbeats. Stroke volume was calculated by dividing the average blood  
183 flow (nL/sec) by the heart beat per second (BPM/60). To assess the heart contractility, movies  
184 were recorded at 120fps and measurements were made using ImageJ software.

185

### 186 **Confocal Imaging**

187 Still images of fixed or anesthetized embryos were recorded using a ProgRes CF colour camera  
188 (Jenoptik) mounted on a SZX16 stereomicroscope (Olympus). Fluorescent embryonic heart  
189 images were acquired with a Leica TCS SP8 inverted confocal laser scanning microscope with  
190 a 20X or 40X oil immersion objectives. Maximal projections and analysis were performed with  
191 Imaris or ImageJ softwares. OFT movements were recorded using a high speed 12kHz resonant  
192 scanner. Image acquisition and image analysis were performed on workstations of the  
193 Montpellier RIO Imaging facility of the Arnaud de Villeneuve/IFR3 campus.

194

### 195 **PCGC data analysis**

196 Whole exomic data for individual probands was downloaded from the NIH/dbGaP repository  
197 (The Pediatric Cardiac Genomics Consortium (PCGC)). The data was subsequently converted

198 into the Fastq format using the SRA toolkit provided by NIH/dbGaP. The exomic data was  
199 aligned to the human reference genome and SNPs associated with *PIEZO1* were identified  
200 using the Integrative Genomics Viewer [14]. Patients' data analysis was approved by the  
201 INSERM Institutional Review Board (IRB00003888 – Opinion number 15-221).

202

### 203 **Real-time quantitative RT-PCR**

204 RNA samples were obtained from 4 dpf larvae. Total RNA was extracted with Trizol  
205 (Invitrogen) and RT-PCR was performed using the Cloned AMV First-Strand cDNA Synthesis  
206 Kit (Invitrogen). For real-time quantitative PCR, we used the SYBR Green I Master (Roche).  
207 Cycling parameters were as follows : 95°C x 10 min, 45 cycles of 95°C x 15 sec and 60°C x 30  
208 sec followed by 95°Cx 10 min. A measure of 10 ng of total RNA was used per reaction.  
209 Quantitative PCR was performed on a Roche LightCycler 480. Samples were run in triplicate.  
210 The primer3 software (<http://www.bioinformatics.nl/cgi-bin/primer3plus/primer3plus.cgi>)  
211 was used to design primers for short amplicon between 100 and 200 bases. Every primers pair  
212 has been verified by Absolute quantification/Fit points and by Tm calling using the LightCycler

tuba1-F        5'-CGGCCAAGCAACACTACTAGA-3'

tuba1-R        5'-AGT TCC CAG CAG GCA TTG-3'

213

Piezo1b-F      5'-AGG AGA AAG CAT TCA GCC CC -3'

Piezo1b-R      5'-CCA GCA GGG GAC TGA ACT TT -3'

Piezo1a-F      5'-ATG ACA TAG GGC CCA GTG GA-3'

Piezo1a-R      5'-TGT CAG CCA GCT GTG ATA CG -3'

214

215 Normalized relative quantification was performed with the  $\Delta\Delta C_t$  method and expression fold  
216 changes were calculated using the following formula :  $e^{(-\Delta\Delta C_t)}$  , using the tubulin alpha1  
217 housekeeping gene as a reference.

218

219

## 220 **References**

- 221 [1] Kwan KM, Fujimoto E, Grabher C, Mangum BD, Hardy ME, Campbell DS, et al. The Tol2kit: a  
222 multisite gateway-based construction kit for Tol2 transposon transgenesis constructs. *Developmental*  
223 *dynamics : an official publication of the American Association of Anatomists.* 2007;236:3088-99.
- 224 [2] Shmukler BE, Huston NC, Thon JN, Ni CW, Kourkoulis G, Lawson ND, et al. Homozygous knockout  
225 of the *piezo1* gene in the zebrafish is not associated with anemia. *Haematologica.* 2015.
- 226 [3] Ranade SS, Qiu Z, Woo SH, Hur SS, Murthy SE, Cahalan SM, et al. *Piezo1*, a mechanically activated  
227 ion channel, is required for vascular development in mice. *Proc Natl Acad Sci U S A.* 2014;111:10347-  
228 52.
- 229 [4] Lukacs V, Mathur J, Mao R, Bayrak-Toydemir P, Procter M, Cahalan SM, et al. Impaired *PIEZO1*  
230 function in patients with a novel autosomal recessive congenital lymphatic dysplasia. *Nat Commun.*  
231 2015;6:8329.
- 232 [5] Fotiou E, Martin-Almedina S, Simpson MA, Lin S, Gordon K, Brice G, et al. Novel mutations in  
233 *PIEZO1* cause an autosomal recessive generalized lymphatic dysplasia with non-immune hydrops  
234 fetalis. *Nat Commun.* 2015;6:8085.
- 235 [6] Rossi A, Kontarakis Z, Gerri C, Nolte H, Holper S, Kruger M, et al. Genetic compensation induced  
236 by deleterious mutations but not gene knockdowns. *Nature.* 2015;524:230-3.
- 237 [7] Stainier DYR, Raz E, Lawson ND, Ekker SC, Burdine RD, Eisen JS, et al. Guidelines for morpholino  
238 use in zebrafish. *PLoS genetics.* 2017;13:e1007000.
- 239 [8] El-Brolosy MA, Kontarakis Z, Rossi A, Kuenne C, Gunther S, Fukuda N, et al. Genetic compensation  
240 triggered by mutant mRNA degradation. *Nature.* 2019;568:193-7.
- 241 [9] Parker T, Libourel PA, Hetheridge MJ, Cumming RI, Sutcliffe TP, Goonesinghe AC, et al. A multi-  
242 endpoint in vivo larval zebrafish (*Danio rerio*) model for the assessment of integrated cardiovascular  
243 function. *J Pharmacol Toxicol Methods.* 2014;69:30-8.
- 244 [10] Kimmel CB, Ballard WW, Kimmel SR, Ullmann B, Schilling TF. Stages of embryonic development  
245 of the zebrafish. *Developmental dynamics : an official publication of the American Association of*  
246 *Anatomists.* 1995;203:253-310.
- 247 [11] Sander JD, Zaback P, Joung JK, Voytas DF, Dobbs D. Zinc Finger Targeter (ZiFiT): an engineered  
248 zinc finger/target site design tool. *Nucleic acids research.* 2007;35:W599-605.
- 249 [12] Jao LE, Wentz SR, Chen W. Efficient multiplex biallelic zebrafish genome editing using a CRISPR  
250 nuclease system. *Proc Natl Acad Sci U S A.* 2013;110:13904-9.
- 251 [13] Goishi K, Lee P, Davidson AJ, Nishi E, Zon LI, Klagsbrun M. Inhibition of zebrafish epidermal  
252 growth factor receptor activity results in cardiovascular defects. *Mechanisms of development.*  
253 2003;120:811-22.
- 254 [14] Robinson JT, Thorvaldsdottir H, Winckler W, Guttman M, Lander ES, Getz G, et al. Integrative  
255 genomics viewer. *Nature biotechnology.* 2011;29:24-6.

256

257

258 **Supplemental figure legends**

259 **Figure S1. Alignment of Piezo1a and Piezo1b.**

260 Protein alignment comparing Piezo1a and Piezo1b.

261

262 **Figure S2. *Piezo1b* is expressed in endothelial cells.**

263 (A-C) ISH using an antisense *piezo1b* probe. (A,B) *Piezo1b* expression can be detected in the  
264 heart of zebrafish embryos (black arrowhead) at 24hpf (A), 48hpf (B). (C) *Piezo1b* is also  
265 expressed in the developing vasculature present on the yolk sac (black arrowhead) and in the  
266 tail (white arrowhead) of 4dpf zebrafish embryos. Double fluorescent ISH using antisense GFP  
267 (D,G) and antisense *piezo1b* (E,H) probes, merged images (F) indicates endothelial GFP and  
268 *piezo1b* co-localise in the endocardium in *Tg(fli1a:GFP)y1* embryos, but not in the  
269 myocardium of *Tg(cmlc2a:GFP)* embryos. V and A in the adjacent cartoon indicate the  
270 ventricle and atrium respectively. Scale bars: (A-C) 100µm, (F, I) 10µm.

271

272 **Figure S3. Pz1b experimental controls.**

273 (A,B) RT-PCR analysis of Pz1b MO1 splice morphant embryos. The Pz1b MO1 targets the  
274 intron 7/exon 8 splice site. Primers designed against exons 7 and 8 (arrows in (A)) are able to  
275 amplify the correct 330bp fragment (lower band in B) from WT embryo cDNA (lane 3). With  
276 morphant embryo cDNA, the final intron has not been spliced out (lane 4) indicating *piezo1b*  
277 has been disrupted. The first two lanes correspond to the negative control without reverse  
278 transcriptase (RT). (C-F) Mouse *Piezo1* RNA can rescue the *piezo1b* morphant phenotype.  
279 Representative images of the severity of cardiac oedema: (C) no oedema, (D) moderate oedema,  
280 (E) severe oedema. (F) Graph indicating the percentage of embryos displaying either no  
281 oedema (white), moderate (grey) or severe (black) in either *piezo1b* morphant embryos (Pz1b  
282 MO) or *piezo1b* morphants co-injected with 20pg of mPz1 RNA (Pz1b MO+Pz1 RNA) n= the

283 cumulative number of embryos from 5 separate experiments. **(G)** Brightfield image of an un-  
284 injected 3dpf *Tg(cmlc2a:GFP)* zebrafish embryo, **(G')** fluorescent image of the same embryo,  
285 GFP can be detected in the heart (green). **(H)** Brightfield image of an Pz1b MO2 injected 3dpf  
286 *Tg(cmlc2a:GFP)* zebrafish embryo, **(H')** Fluorescent image of the same embryo, GFP can be  
287 detected in the heart (green), note the linear appearance of the chambers (n=38/40). **(I,J)** RT-  
288 PCR analysis of Pz1b MO2 morphant embryos. The Pz1b MO2 targets the last intron/exon  
289 splice site **(I)**. Primers designed against the final two exons (arrows in **(I)**) are able to amplify  
290 the correct 440bp fragment (lower band) from wildtype embryo cDNA (lane 1). **(J)** With  
291 morphant embryo cDNA, the final intron has not been spliced out (upper 2,183bp band in lanes  
292 2 and 3) indicating *piezo1b* has been disrupted. **(K)** Brightfield image of a 3dpf embryo injected  
293 with suboptimal (4ng) concentration of Pz1b MO1. **(L)** *In situ* hybridization using an antisense  
294 *cmlc2a* probe indicates heart looping is normal (n=20/20). **(M)** Brightfield image of a 3dpf  
295 embryo injected with suboptimal (3ng) concentration of Pz1b MO2. **(N)** *In situ* hybridization  
296 using an antisense *cmlc2a* probe indicates heart looping is normal (n=20/20). **(O)** Brightfield  
297 image of a 3dpf embryo injected with suboptimal concentration of Pz1b MO1 (4ng) and Pz1b  
298 MO2 (3ng). **(P)** *In situ* hybridization using an antisense *cmlc2a* probe indicates heart looping  
299 is disrupted (n=20/22). **(Q-R)** Mouse *Piezo1* RNA can rescue the *piezo1b* morphant OFT  
300 phenotype. Representative images of the OFT in WT larvae (wt), *piezo1b* morphants (Pz1b  
301 MO) and *piezo1b* morphants co-injected with mPz1 RNA (Pz1bMO+mRNA). The white line  
302 indicates where the width of the OFT was measured. **(R)** Graph indicating the average width of  
303 the OFT in WT (n=10), *piezo1b* morphants (n=10) and *piezo1b* morphants co-injected with  
304 mPiezo1 mRNA (n=12) (\* p<0,05, \*\* p<0.01, student's t-test). **(S,S')** GFP fluorescence in  
305 wildtype *Tg(fli1a:GFP)y1Tg* larvae. White arrow head indicates GFP expressing endocardium.  
306 **(T,T')** GFP fluorescence in *piezo1b* morphant *Tg(fli1a:GFP)y1Tg* larvae. White arrow head  
307 indicates GFP expressing endocardium. **(U)** Confocal maximal projection image of the

308 vasculature in the trunk of a 3dpf un-injected *Tg(fli1a:GFP)y1Tg* transgenic zebrafish embryo.  
309 (V) Confocal maximal projection image of the vasculature in the trunk of a 3dpf Pz1b MO1  
310 injected *Tg(fli1a:GFP)y1Tg* transgenic zebrafish embryo, white arrowheads indicate defects in  
311 vasculature (n=14/15). (Scale bars (G,G',K,L) 100µm.

312

313 **Figure S4. Homozygous *piezo1b<sup>mmr5/mmr5</sup>* knockout zebrafish larvae are compensated.**

314 (A) Brightfield image of a 3dpf *piezo1b<sup>mmr5/mmr5</sup>* zebrafish embryo injected with Pz1b MO. (B)  
315 Brightfield image of a 3dpf *piezo1b<sup>+/+</sup>* zebrafish embryo injected with Pz1b MO (black arrow  
316 head indicates cardiac oedema). (C) Graph depicting the number and genotype of embryos  
317 which did not present a phenotype. Data has been pooled from 2 separate experiments. (D)  
318 Quantitative PCR data indicating that there is no significant change in *piezo1a* gene expression  
319 in *piezo1b<sup>mmr5/mmr5</sup>* zebrafish embryos.

320

321 **Figure S5. *Piezo1b* knockdown perturbs systolic contraction.**

322 (A,B) Representative images of contraction analysis using ImageJ software. The distance  
323 between the two ventricular walls is first measured at the end of diastole (yellow double headed  
324 arrow)(A), (B) the distance is again measured at the end of systole (white double headed arrow,  
325 the difference is indicated by the black double headed arrow).

326

327 **Figure S6. NMDI treatment reveals the compensated phenotype in *piezo1b<sup>mmr5/mmr5</sup>***  
328 **knockout zebrafish larvae.**

329 (A) Representative images of NMDI treated wildtype (WT)(n=20) or *piezo1b<sup>mmr5/mmr5</sup>* zebrafish  
330 larvae. The 4 images of NMDI treated *piezo1b<sup>mmr5/mmr5</sup>* zebrafish larvae depict the range of  
331 severity of the observed phenotype along with percentage of larvae displaying each degree of  
332 severity (n=38). 2 photon images of aortic valves in 7dpf zebrafish larvae labelled with

333 BODIPY. **(A)** Representative image of the aortic valves in a WT larvae, valves are outlined  
334 with a dashed white line (n=8). **(B)** A *piezo1b<sup>mmr5/mmr5</sup>* zebrafish larvae (n=8). Graph depicting  
335 the length to width ratio for the left and right valve leaflets measured in 7dpf WT larvae and  
336 *piezo1b<sup>mmr5/mmr5</sup>* zebrafish larvae. Error bars indicate SD, ANOVA and Dunnet's multiple  
337 comparisons test P<0.01(all samples), student's unpaired homoscedastic two tailed t-test  
338 \*\*P<0.01. Scale bars-20µm.

339

340 **Figure S7. Analysis of *piezo1b* expression in EGFR inhibitor treated zebrafish larvae and**  
341 ***notch1b* KO larvae.**

342 **(A)** *In situ* hybridisation for *piezo1b* in wildtype (WT), wildtype larvae treated with either  
343 AG1478 or PKI166 EGFR inhibitors (WT+AG1478 and WT+PKI166) and *notch1b* KO larvae  
344 (*notch1b<sup>-/-</sup>*) or their WT siblings (*notch1b<sup>+/+</sup>*). Data under relevant images shows the results of  
345 qPCR analysis for *piezo1b* expression performed on larvae from the 3 different conditions.

346

347 **Figure S8. The *fliEP* promoter drives expression in endothelial cells.**

348 Confocal images of *fliEP* driven tdTomato red fluorescent protein in 3dpf zebrafish larvae. **(A)**  
349 Confocal image of the entire vasculature system in a *fliEP:tdTomato* zebrafish larvae. **(B-E)**  
350 Confocal images of the heart of a *fliEP:tdTomato/cmlc2a:GFP* zebrafish larvae. **(B)** tdTomato  
351 is expressed in the endocardium (red). **(C)** GFP is expressed in the surrounding myocardium.  
352 **(D)** Merged image of **(B)+(C)**. **(E)** Image **(D)** merged with a brightfield image. **(F,G)** Confocal  
353 images of the dorsal longitudinal anastomotic vessel (DLAV) of a *fliEP:tdTomato* zebrafish  
354 larvae. **(F)** tdTomato is expressed in the vascular endothelium. **(G)** Image **(F)** merged with a  
355 brightfield image.

356

357 **Movie S1. The beating heart of a 3dpf wildtype embryo.**

358 High speed video recording capturing the beating heart of a 3dpf wildtype embryo. 5 heart beats  
359 are shown at 120fps then the same 5 heart beats are shown at 40fps. Blood can be seen entering  
360 the atrium and passing to the ventricle before ejection.

361

362 **Movie S2. The beating heart of a 3dpf *piezo1b* morphant.**

363 High speed video recording capturing the beating heart of a *piezo1b* morphant. 5 heart beats are  
364 shown at 120fps then the same 5 heart beats are shown at 40fps. Following the contraction of  
365 the ventricle blood can be seen regurgitating back into the atrium.

366

367 **Movie S3. OFT dynamism of a 48hpf *Tg(fli1a:GFP)y1* embryo.**

368 Resonance laser imaging capturing the dynamic movement of the OFT during systole and  
369 diastole. Frames were acquired every 50ms.

370

371 **Movie S4. Dorsal aorta dynamism of a 48hpf *Tg(fli1a:GFP)y1* embryo.**

372 Resonance laser imaging capturing the dynamic movement of the dorsal aorta during systole  
373 and diastole. Frames were acquired every 130ms.

374

375 **Movie S5. Aortic valves in a 7dpf wildtype zebrafish larvae.**

376 2 photon imaging of a BODIPY labelled 7dpf zebrafish larvae reveals the valves dynamically  
377 moving during the cardiac cycle.

378

379 **Movie S6. Aortic valves in a 7dpf *piezo1b* morphant zebrafish larvae.**

380 2 photon imaging of a BODIPY labelled 7dpf *Pz1b* morphant zebrafish larvae reveals the valves  
381 dynamically moving during the cardiac cycle.

382

383 **Movie S7. Aortic valves in a 7dpf *notch1b* mutant zebrafish larvae**

384 2 photon imaging of a BODIPY labelled 7dpf *notch1b* mutant zebrafish larvae reveals the  
385 valves dynamically moving during the cardiac cycle.

386

387 **Movie S8. Echocardiogram of the aortic valve from the Y2022H proband.**

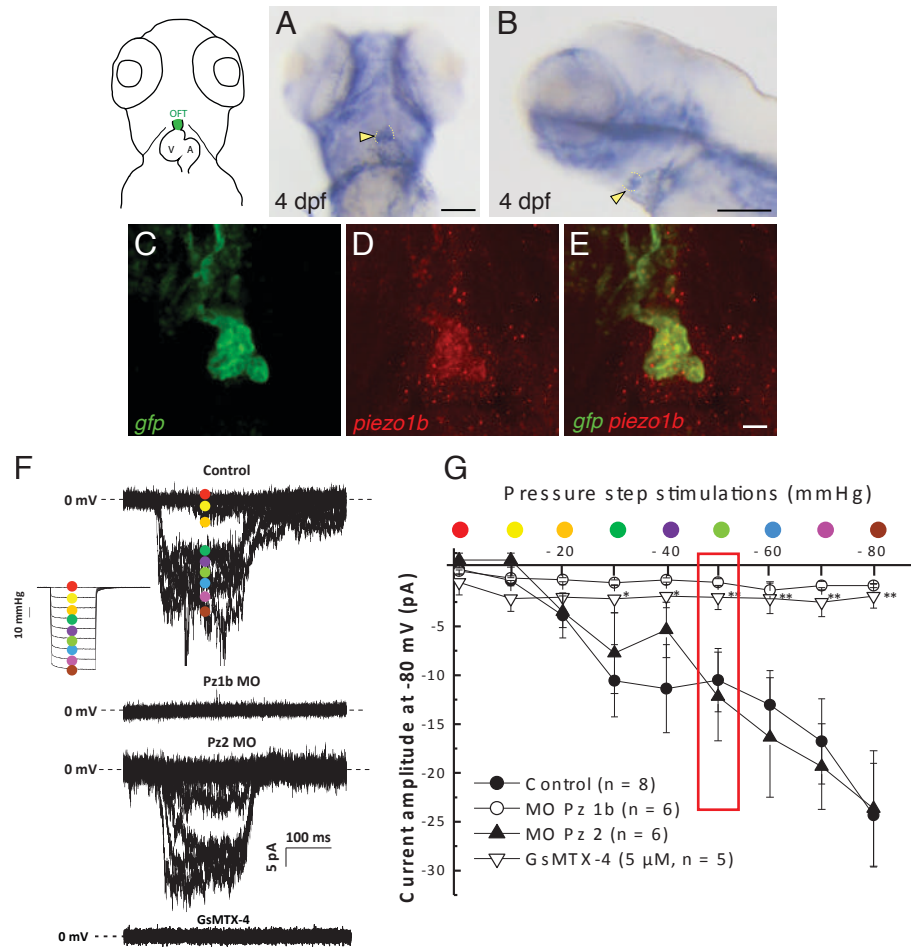
388

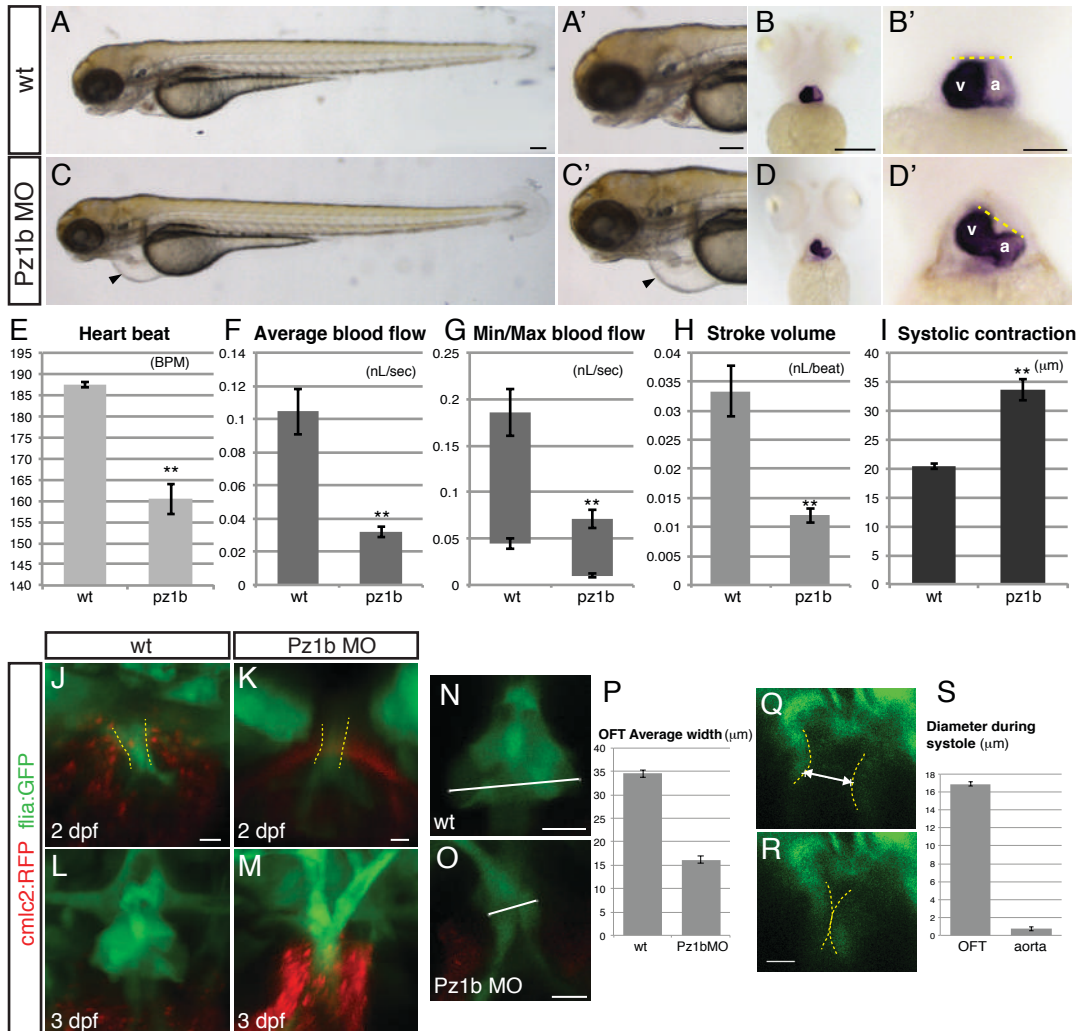
389 **Movie S9. Echocardiogram of the aortic valve from the K2502R proband.**

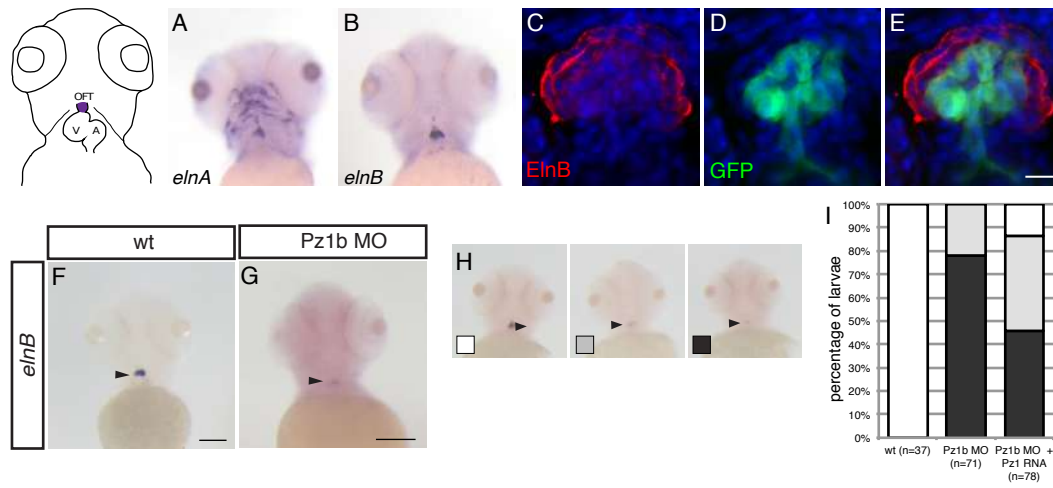
390

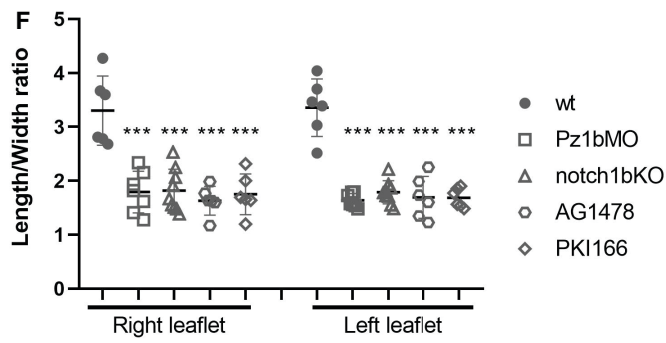
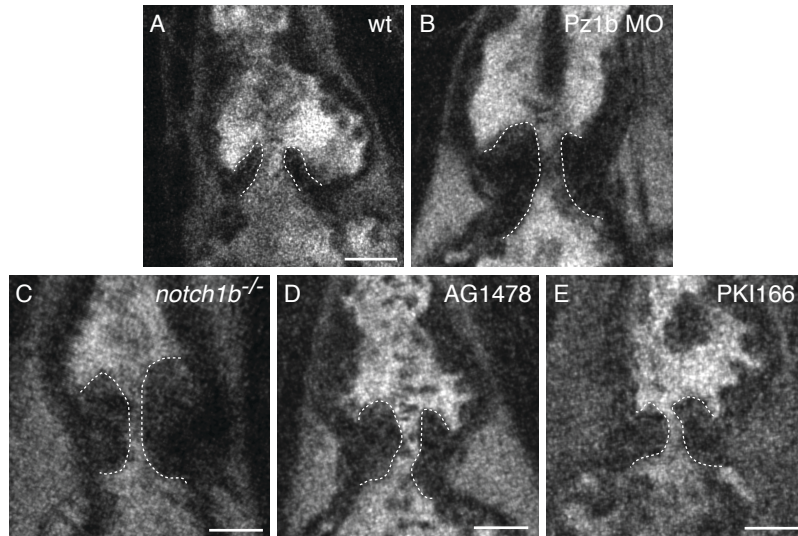
<i>Piezo1</i> mutation	CADD-PHRED	Mutation Taster	UMD Predictor	gnomAD allele frequencies
p.Y2022H (c.6064T>C)	Damaging (27.1)	Damaging (0.58)	Pathogenic (99)	3.336 10 <sup>-5</sup>
p.K2502R (c.7505A>G)	Damaging (25.6)	Damaging (0.80)	Probably pathogenic (69)	6.498 10 <sup>-3</sup>
p.S217L (c.650C>T)	Damaging (25.6)	Damaging (0.54)	Pathogenic (78)	Not reported

**Table.1. Prediction analysis of *PIEZO1* mutations.**

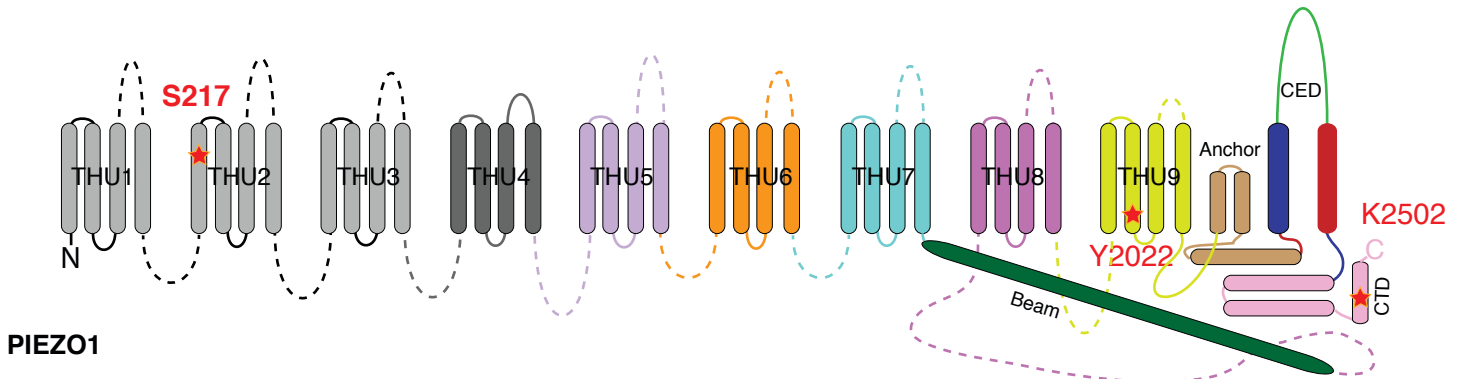




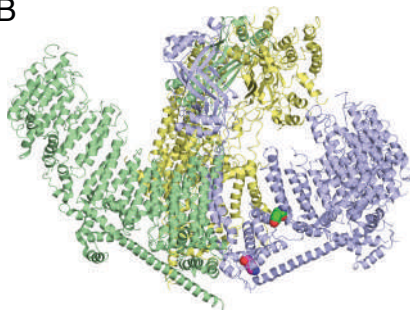




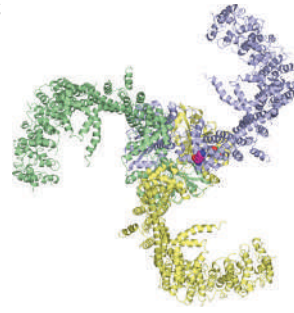
A



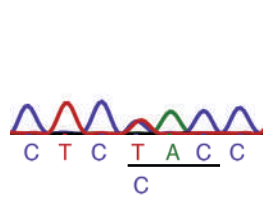
B



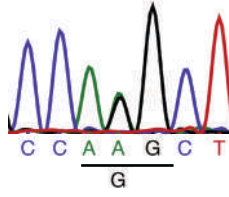
C



D p.Y2022H

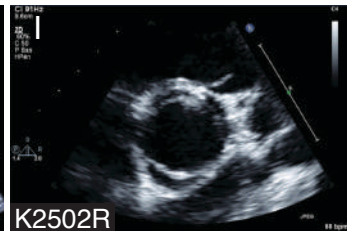


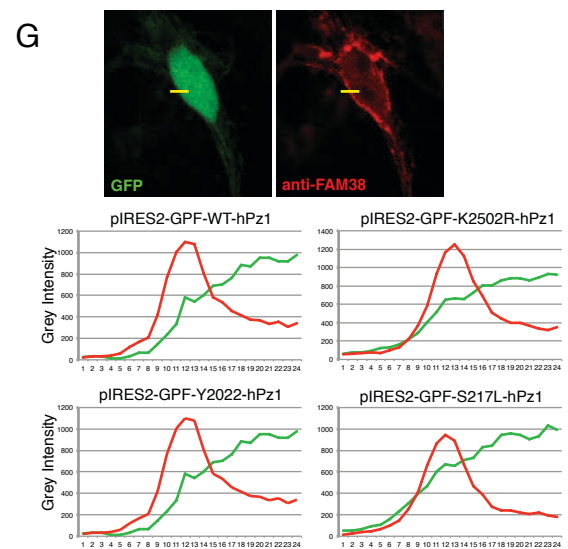
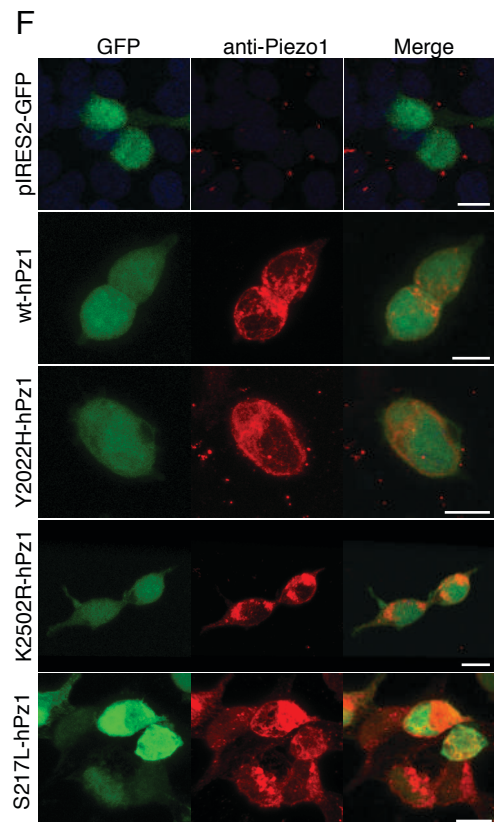
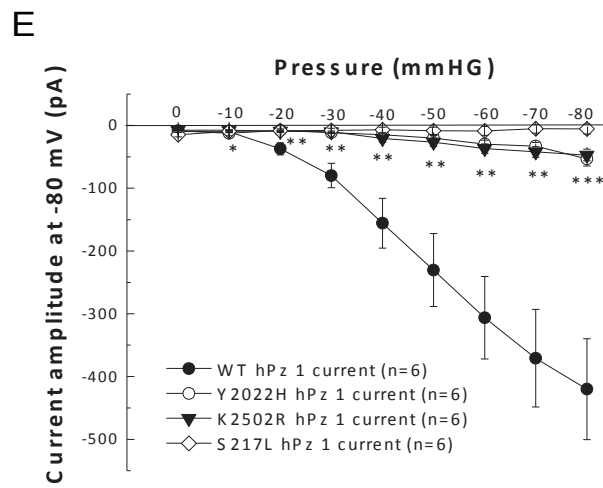
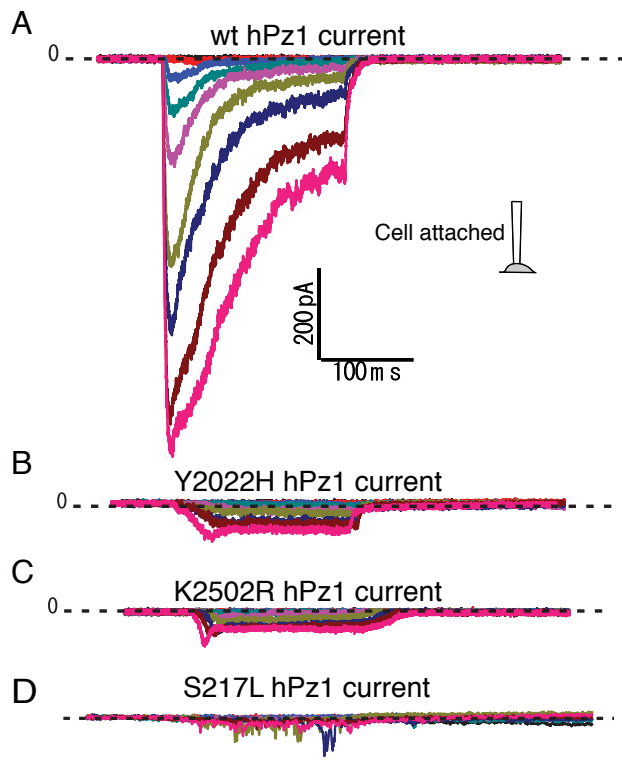
E p.K2502R

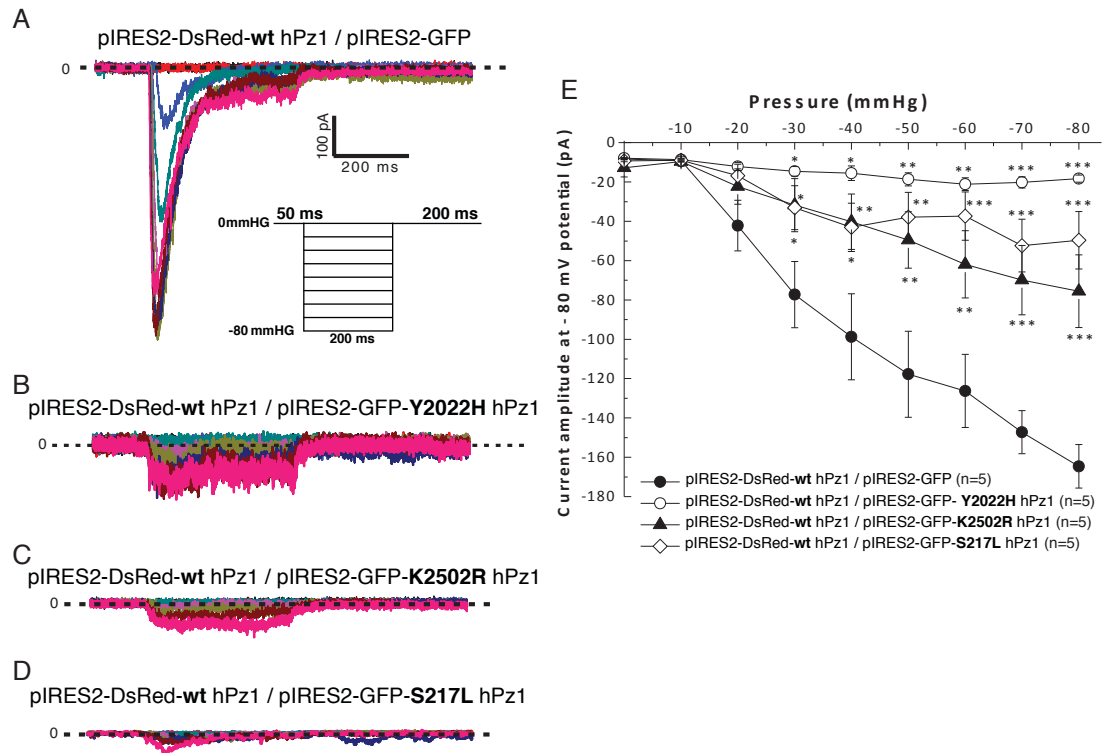


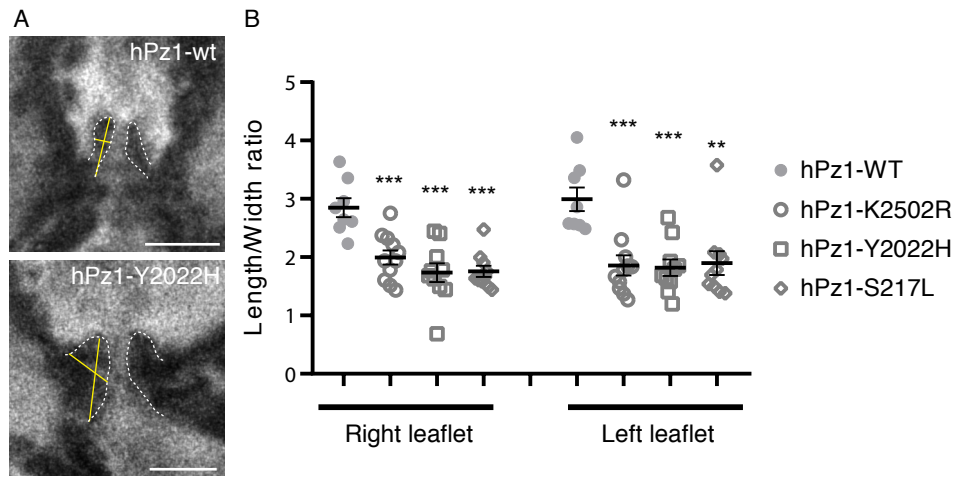
F

	2022	2502	217
human	VDRAL Y LRKTV	EELYA K LIFLY	GIAHP S ALSSV
mouse	IDRAL Y LRKTV	EELYA K LIFLY	GIAHP S AFSSI
chicken	IDRAL Y LRKTV	EELYA K LIFLY	GITLP S ASSSV
zebrafish	VDRAL Y LRKTV	EDLYA K LIFLY	GMMLP S LTSSV
drosophila	IDRAL Y LRKAL	EDLFA K LLFLY	AVLRP S VPGGF
	:**** * ***::	*:*:* * *::***	:: * * ...









Faucherre\_Figure S1

CLUSTAL O(1.2.4) multiple sequence alignment

```

zf_Piezola      MELQVVCGLLYCCLLPIFLLAACIFRYNALSLVYLLYLLLLLPWFQWPNKHTLRGHTGCYI 60
zf_Piezolb      MASELLCGLIFRLLLPVCLAAACLFRYNWLSFVYLVFLLLIPLFAEPHATMTGHTGRLL 60
*   :::***:   ***: * ***:**** **::***::***:* * *.: * : ****  :

zf_Piezola      KALFSTSLIFILGHVTFQICLYTIPSLDDALGHNCSSWETLSRHVGVSRPLLEDPQGVW 120
zf_Piezolb      KVLCLTSVTFLLLHIIFQITVNSLIAGE----- 88
*. *  **: *:* *: *** : :: : :

zf_Piezola      LLTPDLGVFIMSLITLILCSRLKRRDEGSVPHMSALLHEADETEDDEDVEGE-----D 175
zf_Piezolb      SIQPRFNMFVSVLVTWLLCRSLEKPSIKEDSQHNSDFEVDNQEKEDEEEDENREKRELED 148
: *  ::*:***:* **: * * : . * * : : :*.***:** : *      *

zf_Piezola      EGML-----SCSETE--DEE-----SPS-----SSSAAQLAARLRAT 205
zf_Piezolb      ELLFEDFELRDGDCELPENEEEEEAADADDGDLEEDIEESTKTRILRQIADAASKLKEI 208
*  ::          *. *  **:          *.          . * : ***:

zf_Piezola      AQRFLRNMGRILAVTLLALAGITLPSAFSAFYFLFIGVCTWWACHFPISHLGFNALCVM 265
zf_Piezolb      VGNLITSAGKVVVTVLLGLTGMMLPSLTSSVYFFTFGLCTWWSFCRSFDPLLFSCLCVL 268
.  .:: . *:::..**.*:** *** **::***: **::***: : . * *..***:

zf_Piezola      VAFFTGGLVCLYLYQSSFAQAMFSPAGLWARLFGLKDLVTPGNCTTFEVTLNTQYDWPV 325
zf_Piezolb      MAIFSAGHLVFLYLYQFFQEAVPPGNTYASLFGISPVVQTDCSHTWMFKVNPALWVHH 328
*:*:*.**** ***** . * * . *.. :* ***:. :* . . * : ..:* :*

zf_Piezola      YVNPGILLLLYISVTIVLKINSNSLGDADKAREGEAVKTVQGEA-----GEEVELRLW 378
zf_Piezolb      FVNPIMLLVLYYTLATLIRLWLQES EDTVRDAEAEGKDDAASPENTDINVYTADQRRQLW 388
*** **:** ** :: : : : : . * : : *.. . . . : . : **

zf_Piezola      EARRQSSSEDDTK-----QTLL--TTVDSTLS-----ESHITKEPVIN- 413
zf_Piezolb      RMAHYHTDERNLLTAQEAYNSPEVLIVTNSGASLDFTSVSHEKRTKCVERNLYSTPHYKA 448
.  :  :: : .          :*: * : :*:*.          *  :: . *  :

zf_Piezola      GSSQH-----DIGPS-----GEATVDNPLRLVGRMVLQQS YICALIAMMVWS 455
zf_Piezolb      GQPESDTQSLDCGVYRIDSAYVELSELPAVAVRVNSVVKVFRFIMKQSYICALIAMMAWS 508
*. :          * *          .. * : * *:::*****.* **

zf_Piezola      ITYHSWLT FVLLWSCVIWMLRTRQRFAAYCSPFILLYGLALCCLQYVWAMDLETLPQH 515
zf_Piezolb      ITYVSWLTFVFLIWSCTLWVRDRRKYSMVTSPFMVFGNLLIILQYIWSFECLQVPVGL 568
*** *****:***.***: * :::  ***::** * ***:***: : *

zf_Piezola      IGMSLHQLGLDRAQYPCRLRGALLLFTLTFWLLLRQSVKDTFSRKKS-----LTVPLQ 569
zf_Piezolb      FL-----KKEVPPRELGSKTLCLLSFWLLLRQFLTERREKHTDDPQLSDVTVDGH 618
:          : : * .**: * *::***** : : . : : . : **  :

zf_Piezola      EVTTGESTGRNESILKVFGGLVMSLYAKYWIYVCGGMFIMVSFAGKLVAYKIVYMLLFL 629
zf_Piezolb      KLGLQDEAAGHREMMEVLGSSMLAMLNKYWIYICGGMFFVVSFEGRIVMYKIIYMMFLF 678
::  :.. :.***:***. :*: *****:*****:*** *: * ***:***:***:

zf_Piezola      CMCLYQVYYSLWRRLLKAFWMMVVAYTMVVLIAIYTFQFEDFPGYWGNTGFTEQQQLADM 689
zf_Piezolb      CVALYQLHYERWRWMLKYFWMSVVVYTMVLVILVYTFQFESSINVWSNMTGMSREKLEDL 738
*:.***:*. ** **: ** ** **.****:*** :*****. . *.*:***:..* *

zf_Piezola      GLETFKLSELFTSIVIPGFLLACILQLHYFHKPFMKITDLENVSPHHRK-----GID- 743

```



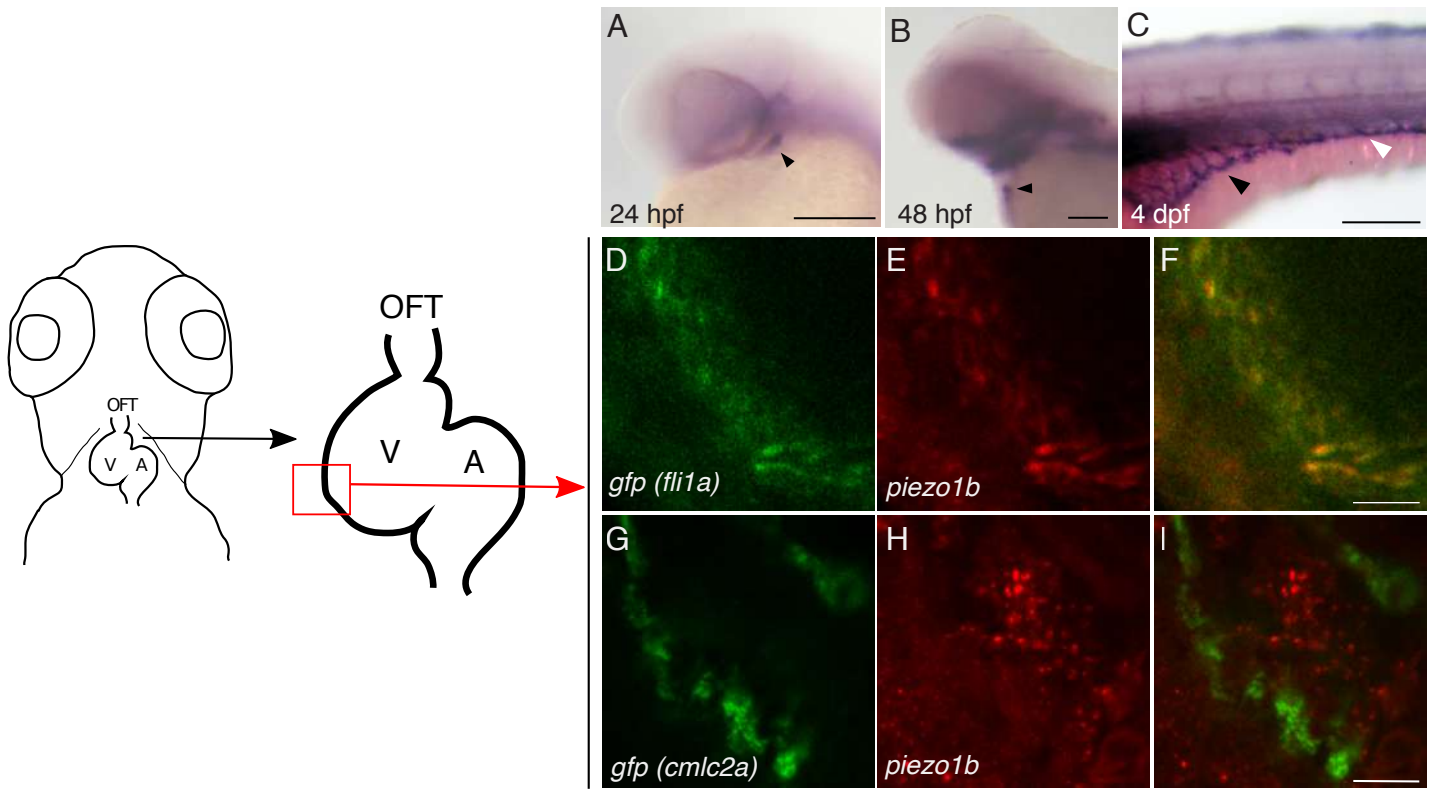


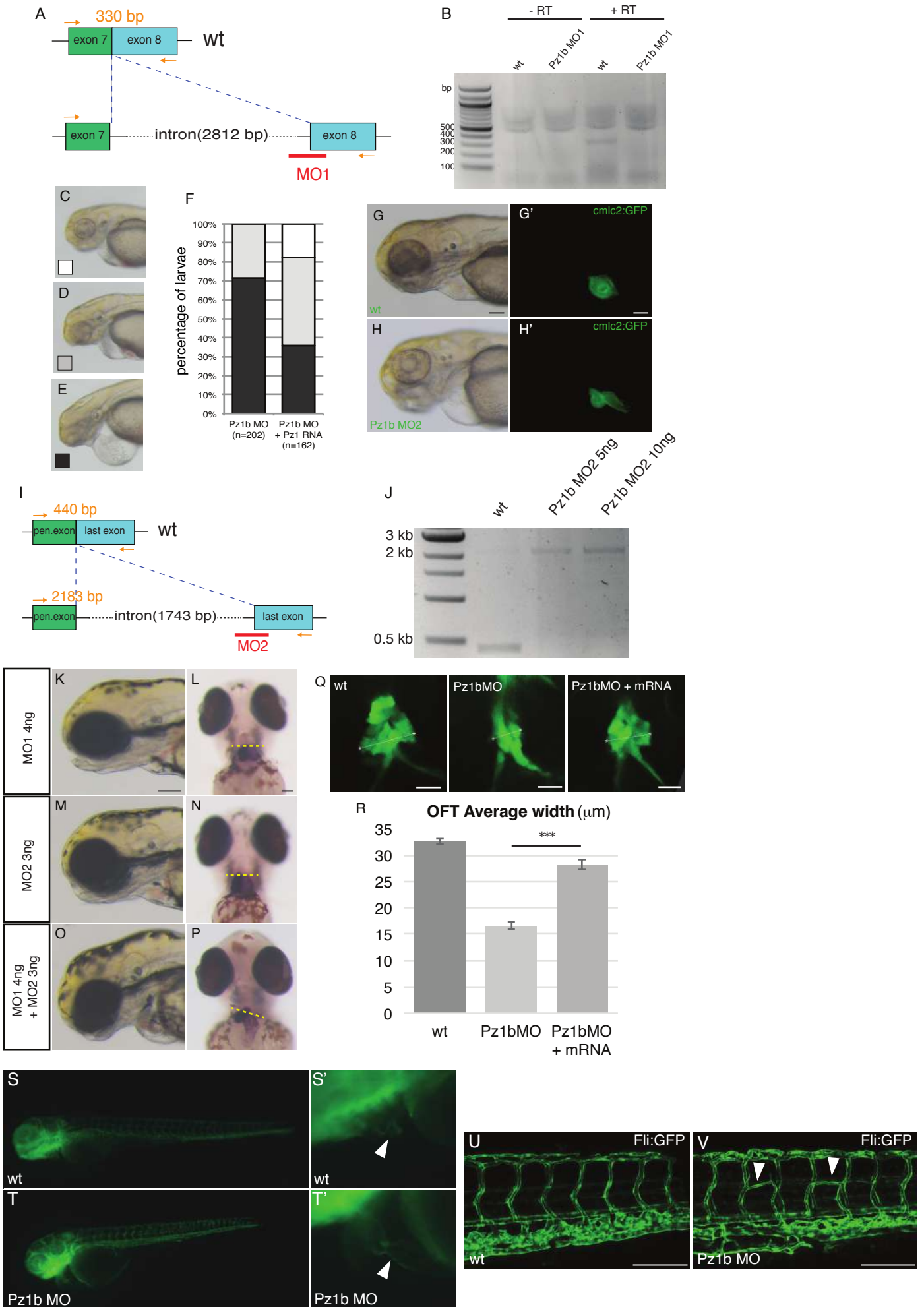
```

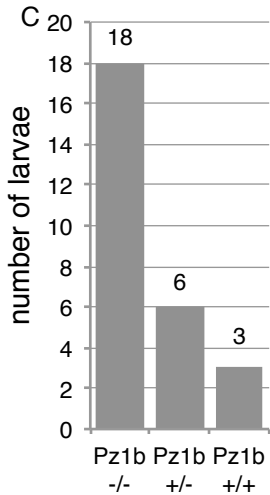
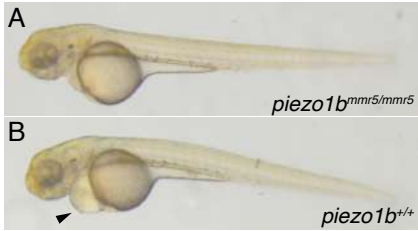
zf_Piezolb      SDFKNFINSYNYVPSAMQFLEAYRAEDVTVAELEGSSNSLWTISPPSRKNLMD-VLSKED 2493
* :::: *:. .      ****: *  **:.*:::**.*:* *****:*.:. :*. .
zf_Piezola      DMTLRLDWNFQRDLDGKGGTVENTFDKHSISLAPKNPVRADLASLLLGTRKDPVHVPHMFP 2372
zf_Piezolb      QFPVTMTWSIQRNLSLGAKAEFAMDKHVTYLDI--KTRQELIALLNGTRNTPVLIQVFP 2551
:: : : *.:**:* . *...* :::** *      .* :* :** ***: ** : :::**
zf_Piezola      NYIRAPSGAEAKPVMQLFDGDEEGFQDVTVSLMREASVNTTGAQEWWDISIAD---CKES 2429
zf_Piezolb      CFIRAPSDSNAKPIEQLYEDGVY--KSIQLDLER-SANSSEDLQEWVIWDELRSAQKQQR 2608
:*****.:***: **:. .      :. :.* * :. :. . **** :.      :.
zf_Piezola      CNVLPMIIFNDKVSPPSLGFLAGYGIMGLYVSVVLVIGKRVGFFSEISHSIMFEELPCA 2489
zf_Piezolb      EAGLQLYVFSDKVSPPSLGFLAGYGIMGLYASVVLVIGKRVREFFSGISHSIMFEELPCV 2668
* : :*.*****.*****.***** ** *****.
zf_Piezola      DRILKLCMDIFLVRETGELELEELYSKLIFLYRSPETMIKWTREKNHN*      2538
zf_Piezolb      DRILKLCMDIFLVRETGELELEEDLYAKLIFLYRSPETMIKWTREKNK*-      2716
***** *****:***:*****:

```

Seq1	Length	Seq2	Length	%Identity
zf_Piezo 1a	2538	zf_Piezo 1b	2716	48.22







D

<b>Fold change</b> ( $e^{(-\Delta\Delta Ct)}$ ) <i>piezo1a</i> expression in <i>piezo1b</i> <sup>-/-</sup> /WT	<b>-0.74</b> (-0.96; +1.67)
---	-----------------------------

